

Left-handed Z' and Z FCNC quark couplings facing new $b \rightarrow s\mu^+\mu^-$ data

Andrzej J. Buras and Jennifer Girrbach

TUM-IAS, Lichtenbergstr. 2a, D-85748 Garching, Germany
 Physik Department, TUM, D-85748 Garching, Germany

Abstract

In view of the recent improved data on $B_{s,d} \rightarrow \mu^+\mu^-$ and $B_d \rightarrow K^*\mu^+\mu^-$ we revisit two simple New Physics (NP) scenarios analyzed by us last year in which new FCNC currents in $b \rightarrow s\mu^+\mu^-$ transitions are mediated either entirely by a neutral heavy gauge boson Z' with purely left-handed complex couplings $\Delta_L^{qb}(Z')$ ($q = d, s$) and real couplings to muons $\Delta_A^{\mu\bar{\mu}}(Z')$ and $\Delta_V^{\mu\bar{\mu}}(Z')$ or the SM Z boson with left-handed complex couplings $\Delta_L^{qb}(Z)$. We demonstrate how the *reduced couplings*, the couplings in question divided by $M_{Z'}$ or M_Z , can be determined by future $\Delta F = 2$ and $b \rightarrow s\mu^+\mu^-$ observables up to sign ambiguities. The latter do not affect the correlations between various observables that can test these NP scenarios. We present the results as functions of $C_{B_q} = \Delta M_q / (\Delta M_q)_{\text{SM}}$, $S_{\psi\phi}$ and $S_{\psi K_S}$ which should be precisely determined in this decade. We calculate the violation of the CMFV relation between $\mathcal{B}(B_{s,d} \rightarrow \mu^+\mu^-)$ and $\Delta M_{s,d}$ in these scenarios. We find that the data on $B_{s,d} \rightarrow \mu^+\mu^-$ from CMS and LHCb can be reproduced in both scenarios but in the case of Z , ΔM_s and $S_{\psi\phi}$ have to be very close to their SM values. As far as $B_d \rightarrow K^*\mu^+\mu^-$ anomalies are concerned the Z' scenario can significantly soften these anomalies while the Z boson fails badly because of the small vector coupling to muons. We also point out that recent proposals of explaining these anomalies with the help of a real Wilson coefficient C_9^{NP} implies uniquely an *enhancement* of ΔM_s with respect to its SM value, while a complex C_9^{NP} allows for both enhancement and suppression of ΔM_s and simultaneously novel CP-violating effects. Correlations between $b \rightarrow s\mu^+\mu^-$ and $b \rightarrow s\nu\bar{\nu}$ observables in these scenarios are emphasized. We also discuss briefly scenarios in which the Z' boson has right-handed FCNC couplings. In this context we point out a number of correlations between angular observables measured in $B_d \rightarrow K^*\mu^+\mu^-$ that arise in the absence of new CP-violating phases in scenarios with only left-handed or right-handed couplings or scenarios in which left-handed and right-handed couplings are equal to each other or differ by sign.

Contents

1	Introduction	1
2	Basic formulae	6
2.1	Basic Lagrangian	6
2.2	$\Delta F = 2$ observables	7
2.3	$b \rightarrow s\mu^+\mu^-$ observables	8
2.4	Correlations between $\Delta M_{s,d}$, $B_{s,d} \rightarrow \mu^+\mu^-$ and C_9^{NP}	10
3	Determining the parameters in the LHS	13
4	Correlations between flavour observables in the LHS	15
4.1	Preliminaries	15
4.2	Strategy	17
4.3	Performing steps 1 and 2	17
4.4	Performing step 3	20
4.5	The $b \rightarrow s\nu\bar{\nu}$ Transitions	27
4.6	Comments on other NP models	28
4.7	Comments on the size of reduced couplings	28
5	The case of the SM Z	29
6	Comments on a real C_9^{NP} and right-handed couplings	33
6.1	Real C_9^{NP}	33
6.2	Right-handed currents	33
7	Conclusions and outlook	43
A	General formulae for correlations	45

1 Introduction

The correlations between flavour observables in concrete New Physics (NP) models are a powerful tool to distinguish between various models and to select the ones that

are consistent with the data [1]. Among prominent examples where such correlations are rather stringent are models with constrained minimal flavour violation (CMFV) [2, 3], MFV at large [4–6], GMFV [7], models with $U(2)^3$ flavour symmetry [8–11] and supersymmetric models with flavour symmetries [12].

Also models in which all FCNCs are mediated entirely by a neutral gauge boson Z' imply a multitude of correlations as analyzed in detail in [13–17]. A review of Z' models can be found in [18] and other recent studies in these models have been presented in [19–24].

While FCNC Z' couplings to quarks could be generally left-handed and right-handed, as demonstrated in particular in [14], a very interesting scenario is the LHS one in which Z' couplings to quarks are purely left-handed. The nice virtue of this scenario is that for certain choices of the Z' couplings the model resembles the structure of CMFV or models with $U(2)^3$ flavour symmetry. Moreover as no new operators beyond those present in the SM are present, the non-perturbative uncertainties are the same as in the SM, still allowing for non-MFV contributions beyond those present in $U(2)^3$ models. In particular the stringent CMFV relation between $\Delta M_{s,d}$ and $\mathcal{B}(B_{s,d} \rightarrow \mu^+ \mu^-)$ [25] valid in the simplest $U(2)^3$ models is violated in the LHS scenario as we will see below.

Another virtue of the LHS scenario is the paucity of its parameters that enter all flavour observables in a given meson system which should be contrasted with most NP scenarios outside the MFV framework. Indeed, if we concentrate on $B_s^0 - \bar{B}_s^0$ mixing, $b \rightarrow s\mu^+\mu^-$ and $b \rightarrow s\nu\bar{\nu}$ observables there are only four new parameters to our disposal: the three *reduced couplings* of which the first one is generally complex and the other two real. These are (our normalizations of couplings are given in Section 2)

$$\bar{\Delta}_L^{sb}(Z') = \frac{\Delta_L^{sb}(Z')}{M_{Z'}}, \quad \bar{\Delta}_A^{\mu\bar{\mu}}(Z') = \frac{\Delta_A^{\mu\bar{\mu}}(Z')}{M_{Z'}}, \quad \bar{\Delta}_V^{\mu\bar{\mu}}(Z') = \frac{\Delta_V^{\mu\bar{\mu}}(Z')}{M_{Z'}}, \quad (1)$$

where the *bar* distinguishes these couplings from the ones used in [14]. The couplings $\Delta_{A,V}^{\mu\bar{\mu}}(Z')$ are defined in (11) and due to $SU(2)_L$ symmetry implying in LHS $\Delta_L^{\nu\bar{\nu}}(Z') = \Delta_L^{\mu\bar{\mu}}(Z')$ one also has

$$\Delta_L^{\nu\bar{\nu}}(Z') = \frac{\Delta_V^{\mu\bar{\mu}}(Z') - \Delta_A^{\mu\bar{\mu}}(Z')}{2}. \quad (2)$$

Concrete models satisfying this relation are the 3-3-1 models analyzed in [13]. This relation has also been emphasized recently in [26, 27].

The four new parameters in (1) describe in this model NP effects in flavour violating processes, in particular

$$\Delta M_s, \quad S_{\psi\phi}, \quad B_s \rightarrow \mu^+\mu^-, \quad S_{\mu\mu}^s, \quad B \rightarrow K\nu\bar{\nu}, \quad B \rightarrow K^*\nu\bar{\nu}, \quad B \rightarrow X_s\nu\bar{\nu}. \quad (3)$$

and

$$B_d \rightarrow K\mu^+\mu^-, \quad B_d \rightarrow K^*\mu^+\mu^-, \quad B_d \rightarrow X_s\mu^+\mu^-. \quad (4)$$

Extending these considerations to $B_d^0 - \bar{B}_d^0$ mixing and $B_d \rightarrow \mu^+\mu^-$ we have to our disposal presently

$$\Delta M_d, \quad S_{\psi K_S}, \quad B_d \rightarrow \mu^+\mu^-. \quad (5)$$

It should be noted that in these three observables only $\bar{\Delta}_L^{db}(Z')$ is new as the muon couplings $\bar{\Delta}_{A,V}^{\mu\bar{\mu}}(Z')$ are already determined through the observables (3) and (4).

In [14] a very detailed analysis of the correlations among observables in (3) and among the ones in (5) has been presented taking into account the constraints from the processes (4) known at the time of our analysis. In the meantime two advances on the experimental side have been made that deal with processes listed above:

- The LHCb and CMS collaborations presented new results on $B_{s,d} \rightarrow \mu^+\mu^-$ [28–30]. While the branching ratio for $B_s \rightarrow \mu^+\mu^-$ turns out to be rather close to SM prediction, although a bit lower, the central value for the one of $B_d \rightarrow \mu^+\mu^-$ is by a factor of 3.5 higher than its SM value.
- LHCb collaboration reported new results on angular observables in $B_d \rightarrow K^*\mu^+\mu^-$ that show significant departures from SM expectations [31, 32]. Moreover, new data on the observable F_L , consistent with LHCb value in [31] have been presented by CMS [33].

In particular the anomalies in $B_d \rightarrow K^*\mu^+\mu^-$ triggered recently two sophisticated analyses [26, 34] with the goal to understand the data and to indicate what type of new physics could be responsible for these departures from the SM. Both analyses point toward NP contributions in the modified coefficients $C_{7\gamma}$ and C_9 with the following shifts with respect to their SM values:

$$C_{7\gamma}^{\text{NP}} < 0, \quad C_9^{\text{NP}} < 0. \quad (6)$$

Other possibilities, in particular involving right-handed currents, have been discussed in [26]. It should be emphasized at this point that these analyses are subject to theoretical uncertainties, which have been discussed at length in [34–38] and it remains to be seen whether the observed anomalies are only result of statistical fluctuations and/or underestimated error uncertainties. Assuming that this is not the case we will investigate how LHS faces these data.

As far as C_9^{NP} is concerned, the favorite scenario suggested in [34] is precisely the LHS scenario analyzed in [14] but with a simplifying assumption that C_9^{NP} is real. In [34] it has also been suggested that $\Delta_A^{\mu\bar{\mu}}(Z') \approx 0$ and in fact also in the examples of Z' models presented in [26, 27] the axial-vector coupling has been set to zero. Clearly such a solution, as already mentioned in these papers, would eliminate NP contributions to $B_s \rightarrow \mu^+\mu^-$ which although consistent with the present data is not particularly interesting. We would like to add that such a choice would also eliminate NP contributions to $B_d \rightarrow \mu^+\mu^-$ precluding the explanation in LHS of a possible enhancement of $\mathcal{B}(B_d \rightarrow \mu^+\mu^-)$ indicated by the LHCb and CMS data.

It should be remarked that according to the analysis in [26] C_9^{NP} , while reducing significantly the anomalies in the angular observables S_5 and F_L , cannot provide a complete solution when the data on $B \rightarrow K\mu^+\mu^-$ and the forward-backward asymmetry A_{FB} are taken into account. Yet the nice pattern that a negative C_9^{NP} automatically shifts S_5 and F_L in the right direction towards the data is a virtue of this simple scenario.

The inclusion of a negative NP contribution $C_{7\gamma}^{\text{NP}}$, which exhibits the same pattern in the shifts in S_5 and F_L , together with C_9^{NP} would provide a better fit to the data. However in the context of our general analysis in [14] we have demonstrated that the contribution of Z' to $C_{7\gamma}$ is fully negligible. Whether this is a problem for LHS remains to be seen when the data on $B_d \rightarrow K^*\mu^+\mu^-$ and $B \rightarrow X_s\gamma$ improve. Thus indeed in what follows we can concentrate on modifications in two Wilson coefficients, C_9 and C_{10} , that are relevant for flavour observables in $B_d \rightarrow K^*\mu^+\mu^-$ and $B_s \rightarrow \mu^+\mu^-$, respectively.

Having developed the full machinery for analyzing the processes in question in Z' models in [14] we would like in this paper to have still another look at the LHS scenario in view of the most recent data. As already two detailed analyses of anomalies in $B_d \rightarrow K^*\mu^+\mu^-$ have been presented in [26, 34], our paper will be dominated by $B_{s,d} \rightarrow \mu^+\mu^-$ decays. Therefore, in contrast to these papers the vector-axial coupling $\Delta_A^{\mu\bar{\mu}}(Z')$ will play a crucial role in our analysis. In particular in the spirit of [1, 14] we will expose in the LHS the correlations between $\Delta F = 2$ observables and $B_{s,d} \rightarrow \mu^+\mu^-$ illustrating their dependence on $\Delta M_{s,d}/(\Delta M_{s,d})_{\text{SM}}$, $S_{\psi\phi}$ and $S_{\psi K_S}$ which should be precisely determined in this decade. Here the theoretically clean CMFV relation between these observables [25], that is violated in the LHS, will play a prominent role. However, we will also briefly discuss the correlation between ΔM_s and the size of C_9^{NP} necessary to understand the $B_d \rightarrow K^*\mu^+\mu^-$ anomalies [26, 34].

Now, in [14] we have performed already a very detailed analysis of the processes and observables listed in (3) and (5) in the LHS scenario and it is mandatory for us to state what is new in the present paper:

- First of all the data on $B_{s,d} \rightarrow \mu^+\mu^-$ changed relative to those known at the time of the analysis in [14] and we would like to confront LHS with these data. In particular as stated above we will calculate the deviations from the stringent CMFV relation between $\Delta M_{s,d}$ and $\mathcal{B}(B_{s,d} \rightarrow \mu^+\mu^-)$ [25] present in this model that has not been done in [14] nor in any other paper known to us. An exception is our analysis of 3-3-1 models in [13] but in this concrete Z' model NP effects in $B_d \rightarrow \mu^+\mu^-$ are too small to reproduce the recent data within 1σ .
- While in [14] we have demonstrated how the coupling $\Delta_L^{sb}(Z')$ could be determined from ΔM_s , $S_{\psi\phi}$ and $B_s \rightarrow \mu^+\mu^-$ observables and the coupling $\Delta_L^{db}(Z')$ from ΔM_d , $S_{\psi K_S}$ and $B_d \rightarrow \mu^+\mu^-$, we have done it for chosen values of the muon coupling $\Delta_A^{\mu\bar{\mu}}(Z')$ and $M_{Z'}$ and using in particular the CP-asymmetry $S_{\mu\mu}^s$ which is very difficult to measure. In the present paper we want to summarize how the three reduced couplings listed in (1) can be determined by invoking in addition the

angular observables in $B_d \rightarrow K^* \mu^+ \mu^-$ that can be much easier measured than $S_{\mu\mu}^s$ and not making a priori any assumptions on $\Delta_{A,V}^{\mu\bar{\mu}}(Z')$ and $M_{Z'}$

- In view of the continued progress in lattice calculations we will investigate how the results presented here depend on the values of C_{B_s} and C_{B_d} whose departure from unity measures the NP effects in ΔM_s and ΔM_d . We will see that precise knowledge of these parameters as well as precise measurements of CP-asymmetries $S_{\psi\phi}$ and $S_{\psi K_S}$ are very important for the determination of the couplings in (1).
- We will refine our previous analysis of the correlations of $B_s \rightarrow \mu^+ \mu^-$ and $b \rightarrow s\nu\bar{\nu}$ observables.
- In the context of our presentation we will critically analyze the LHS scenario with a real coefficient C_9^{NP} advocated in [26,34]. In particular we present a correlation between real C_9^{NP} and ΔM_s pointing out that in LHS ΔM_s is then uniquely enhanced which could be tested one day when lattice calculations and values of CKM parameters will be more precise. We discuss briefly the implications of such a scenario for $B_s \rightarrow \mu^+ \mu^-$, $S_{\psi\phi}$ and $b \rightarrow s\nu\bar{\nu}$ transitions.
- We point out a number of correlations between angular observables in $B_d \rightarrow K^* \mu^+ \mu^-$ which arise in LHS, RHS, LRS and ALRS scenarios for couplings of [14] when new CP-violating phases are neglected.
- As far as Z -scenario is concerned we note that large enhancement of $\mathcal{B}(B_d \rightarrow \mu^+ \mu^-)$ found by us in [14] is fully consistent with the recent LHCb and CMS data. However, this scenario does not allow the explanation of the $B_d \rightarrow K^* \mu^+ \mu^-$ anomalies when the constraint from ΔM_s is taken into account. Due to the smallness of the vector coupling of Z to muons the required modification of C_9 implies in this scenario shifts in ΔM_s and in C_{10} that are by far too large.

Our paper is organized as follows. In Section 2 we summarize the basic formulae used in our analysis referring often to the expressions in [14], where the same notation is used. In Section 3 we show a simple procedure for the determination of the reduced couplings in (1) up to their signs. In Section 4, the most important section of our paper, we perform an anatomy of correlations between $B_{s,d}^0 - \bar{B}_{s,d}^0$ and $B_{s,d} \rightarrow \mu^+ \mu^-$ observables taking into account the information from $B_d \rightarrow K^* \mu^+ \mu^-$ decay. We also include $b \rightarrow s\nu\bar{\nu}$ in this discussion. In Section 5 we consider the case of the SM Z gauge boson with FCNC couplings. In this case the leptonic reduced couplings are fixed. In Section 6 we address the case of a real C_9 , the enhancement of ΔM_s in this case and of the implications for other observables. We also discuss briefly scenarios in which Z' and Z have also right-handed FCNC couplings and point out a number of correlations between angular observables in $B_d \rightarrow K^* \mu^+ \mu^-$ advertised above. We conclude in Section 7.

Before starting our presentation let us realize that the challenges the LHS scenario considered in our paper has to face are non-trivial due to the following facts.

The important actors in our paper are the couplings

$$\bar{\Delta}_L^{sb}(Z'), \quad \bar{\Delta}_L^{db}(Z'), \quad \bar{\Delta}_A^{\mu\bar{\mu}}(Z'), \quad \bar{\Delta}_V^{\mu\bar{\mu}}(Z'), \quad (7)$$

in terms of which the decays and related observables in (3)-(5) should be simultaneously described. In view of the pattern of the present data mentioned above this is certainly non-trivial for the following reasons:

- $\bar{\Delta}_L^{sb}(Z')$ enters both $B_s \rightarrow \mu^+\mu^-$ and $B_d \rightarrow K^*\mu^+\mu^-$ in which NP effects have been found to be small and sizable, respectively. This implies through the relation (24) that $\bar{\Delta}_A^{\mu\bar{\mu}}(Z') < \bar{\Delta}_V^{\mu\bar{\mu}}(Z')$.
- The smallness of $\bar{\Delta}_L^{sb}(Z')$ is welcome as then also NP effects in ΔM_s are small as seen in the data. But then $\bar{\Delta}_V^{\mu\bar{\mu}}(Z')$ must be sufficiently large in order to describe the anomalies in $B_d \rightarrow K^*\mu^+\mu^-$.
- Similarly $\bar{\Delta}_A^{\mu\bar{\mu}}(Z')$ cannot be small, in spite of $B_s \rightarrow \mu^+\mu^-$ being SM-like as otherwise the enhancement of $B_d \rightarrow \mu^+\mu^-$ branching ratio over SM expectation indicated by the LHCb and CMS data cannot be accommodated. Here the sizable coupling $\bar{\Delta}_L^{db}(Z')$ could help, but it is constrained by ΔM_d and $S_{\psi K_S}$.
- In the Z -scenario the challenges are even larger as the lepton couplings are fixed.

We are now ready to investigate how LHS Z' and Z scenarios face these challenges.

2 Basic formulae

2.1 Basic Lagrangian

The basic formalism for our analysis has been developed in [14] and we collect here only those formulae of that paper that are essential for our presentation expressing them this time in terms of the reduced couplings in (1). However we recall first the basic Lagrangian in terms of the couplings used in [14] ($q = d, s$):

$$\mathcal{L}_{\text{FCNC}}^{\text{quarks}}(Z') = \left[\bar{q}\gamma_\mu P_L b \Delta_L^{qb}(Z') + \bar{q}\gamma_\mu P_R b \Delta_R^{qb}(Z') + h.c. \right] Z'^\mu, \quad (8)$$

$$\mathcal{L}^{\text{leptons}}(Z') = \left[\bar{\mu}\gamma_\mu P_L \mu \Delta_L^{\mu\bar{\mu}}(Z') + \bar{\mu}\gamma_\mu P_R \mu \Delta_R^{\mu\bar{\mu}}(Z') + \bar{\nu}\gamma_\mu P_L \Delta_L^{\nu\bar{\nu}}(Z') \right] Z'^\mu \quad (9)$$

where R and L stand for right-handed and left-handed couplings $\gamma_\mu(1 \pm \gamma_5)/2$. Moreover

$$\bar{\Delta}_L^{bq}(Z') = \left[\bar{\Delta}_L^{qb}(Z') \right]^* \quad (10)$$

and the vector and axial-vector couplings to muons are given as follows

$$\begin{aligned}\Delta_V^{\mu\bar{\mu}}(Z') &= \Delta_R^{\mu\bar{\mu}}(Z') + \Delta_L^{\mu\bar{\mu}}(Z'), \\ \Delta_A^{\mu\bar{\mu}}(Z') &= \Delta_R^{\mu\bar{\mu}}(Z') - \Delta_L^{\mu\bar{\mu}}(Z').\end{aligned}\tag{11}$$

The relation of these couplings to the ones used in [26] is as follows

$$\bar{\Delta}_{L,R}^{qb}(Z') = \frac{g_2}{2 \cos \theta_W} g_{qb}^{L,R}, \quad \Delta_{V,A}^{\mu\bar{\mu}}(Z') = \frac{g_2}{\cos \theta_W} g_{\mu}^{V,A},\tag{12}$$

where g_2 is the $SU(2)_L$ gauge coupling. For completeness and because of a brief discussion in Section 6 we have included here right-handed couplings $\bar{\Delta}_R^{qb}(Z')$ which vanish in the LHS.

On the other hand we do not make any assumptions about diagonal couplings of Z' to quarks but we expect them to be non-vanishing. The flavour violating couplings in the quark mass eigenstate basis can e.g. arise from the non-universality of the diagonal couplings in the flavour basis but other dynamical mechanisms for the FCNC couplings in question are possible [18]. Without a concrete model it is not possible to establish a relation between diagonal and non-diagonal couplings. For a recent discussion see [39] and references therein.

2.2 $\Delta F = 2$ observables

The $B_s^0 - \bar{B}_s^0$ observables are fully described in LHS by the function

$$S(B_s) = S_0(x_t) + \Delta S(B_s) \equiv |S(B_s)| e^{-i2\varphi_{B_s}},\tag{13}$$

where $S_0(x_t)$ is the real one-loop SM box function and the additional generally complex term, denoted in [14] by $[\Delta S(B_s)]_{\text{VLL}}$, is the tree-level Z' contribution

$$\Delta S(B_s) = \left[\frac{\bar{\Delta}_L^{bs}(Z')}{V_{tb}^* V_{ts}} \right]^2 \frac{4\tilde{r}}{g_{\text{SM}}^2}, \quad g_{\text{SM}}^2 = 4 \frac{G_F}{\sqrt{2}} \frac{\alpha}{2\pi \sin^2 \theta_W}.\tag{14}$$

Here \tilde{r} is a QCD factor that includes QCD renormalization group effects between $\mu = M_{Z'}$ and $\mu = m_t$ and the difference in matching conditions between full and effective theories in the tree-level Z' exchanges [40] and SM box diagrams [41]. Explicit expression for \tilde{r} has been given in [13]. One finds $\tilde{r} = 0.985$, $\tilde{r} = 0.953$ and $\tilde{r} = 0.925$ for $M_{Z'} = 1, 3, 10$ TeV, respectively.

The two observables of interest, ΔM_s and $S_{\psi\phi}$ are then given by

$$\Delta M_s = \frac{G_F^2}{6\pi^2} M_W^2 m_{B_s} |V_{tb}^* V_{ts}|^2 F_{B_s}^2 \hat{B}_{B_s} \eta_B |S(B_s)|\tag{15}$$

and

$$S_{\psi\phi} = \sin(2|\beta_s| - 2\varphi_{B_s}), \quad V_{ts} = -|V_{ts}| e^{-i\beta_s}.\tag{16}$$

with $\beta_s \simeq -1^\circ$.

In the case of B_d^0 system the corresponding formulae are obtained from (13)-(15) by replacing s by d . Moreover (16) is replaced by

$$S_{\psi K_S} = \sin(2\beta - 2\varphi_{B_d}), \quad V_{td} = |V_{td}|e^{-i\beta}. \quad (17)$$

The value of β depends strongly on $|V_{ub}|$ but only weakly on its phase γ . For $\gamma = 68^\circ$ we find $\beta = 21.2^\circ$ and $\beta = 25.2^\circ$ for $|V_{ub}| = 3.4 \times 10^{-3}$ and $|V_{ub}| = 4.0 \times 10^{-3}$, respectively.

It should be noted that $M_{Z'}$ is hidden in the reduced $Z'bs$ coupling and appears explicitly only in \tilde{r} but this dependence is only logarithmic and can be neglected in view of present theoretical and experimental uncertainties but should be taken into account in the flavour precision era. However, except for this weak dependence at tree level it is not possible to measure $M_{Z'}$ through FCNC processes unless the relevant couplings are predicted in a given model. On the other hand it could be in principle possible through loop processes one day or through direct high energy experiments that would discover Z' .

2.3 $b \rightarrow s\mu^+\mu^-$ observables

The two Wilson coefficients that receive NP contributions in LHS model are C_9 and C_{10} . We decompose them into the SM and NP contributions¹:

$$C_9 = C_9^{\text{SM}} + C_9^{\text{NP}}, \quad C_{10} = C_{10}^{\text{SM}} + C_{10}^{\text{NP}}. \quad (18)$$

Then [14]²

$$\sin^2 \theta_W C_9^{\text{SM}} = \sin^2 \theta_W P_0^{\text{NDR}} + [\eta_Y Y_0(x_t) - 4 \sin^2 \theta_W Z_0(x_t)], \quad (19)$$

$$\sin^2 \theta_W C_{10}^{\text{SM}} = -\eta_Y Y_0(x_t) \quad (20)$$

so that

$$C_9^{\text{SM}} \approx 4.1, \quad C_{10}^{\text{SM}} \approx -4.1. \quad (21)$$

NP contributions have a very simple structure

$$\sin^2 \theta_W C_9^{\text{NP}} = -\frac{1}{g_{\text{SM}}^2} \frac{\bar{\Delta}_L^{sb}(Z') \bar{\Delta}_V^{\mu\bar{\mu}}(Z')}{V_{ts}^* V_{tb}}, \quad (22)$$

$$\sin^2 \theta_W C_{10}^{\text{NP}} = -\frac{1}{g_{\text{SM}}^2} \frac{\bar{\Delta}_L^{sb}(Z') \bar{\Delta}_A^{\mu\bar{\mu}}(Z')}{V_{ts}^* V_{tb}}. \quad (23)$$

¹These coefficients are defined as in [14] and the same definitions are used in [26, 34].

²The quantities η_Y , η_B and η_X appearing in the text are QCD corrections for which the values, all $\mathcal{O}(1)$, can be found in [14].

and consequently we have an important relation

$$\frac{C_{10}^{\text{NP}}}{C_9^{\text{NP}}} = \frac{\bar{\Delta}_A^{\mu\bar{\mu}}(Z')}{\bar{\Delta}_V^{\mu\bar{\mu}}(Z')}, \quad (24)$$

which involves only leptonic couplings.

$Y_0(x_t)$ and $Z_0(x_t)$ are SM one-loop functions, analogous to $S_0(x_t)$. Explicit expressions for them can be found in [14]. C_{10} is scale independent as far as pure QCD corrections are concerned but at higher order in QED the relevant operator mixes with other operators [42, 43]. This effect will be included in the complete calculation of NLO electroweak corrections to $B_s \rightarrow \mu^+\mu^-$. C_9 is affected by QCD corrections, present in the term P_0^{NDR} , through mixing with four-quark current-current operators. Its value is usually quoted at $\mu = \mathcal{O}(m_b)$. Beyond one-loop this term is renormalization scheme dependent but as demonstrated in [44] at the NLO level this dependence is canceled by QCD corrections to the matrix elements of the relevant operators. By now these corrections are known at the NNLO level [42, 45, 46] and are taken into account in the extraction of C_9^{NP} from the data. Finally, it should be mentioned that there are also QCD corrections affecting the NP part due to the mixing of new four-quark operators generated through Z' exchange. These corrections would effectively modify the term P_0^{NDR} . Corrections of this type have been calculated in the case of Z' contributions to $B \rightarrow X_s\gamma$ decay in [14, 47] and found to be small. As the anomalous dimensions in the present case are smaller than in the case of $B \rightarrow X_s\gamma$ it is safe to neglect these corrections.

One has then in the case of $B_s \rightarrow \mu^+\mu^-$ decay [16, 48, 49]

$$\frac{\bar{\mathcal{B}}(B_s \rightarrow \mu^+\mu^-)}{\bar{\mathcal{B}}(B_s \rightarrow \mu^+\mu^-)_{\text{SM}}} = \left[\frac{1 + \mathcal{A}_{\Delta\Gamma}^{\mu\mu} y_s}{1 + y_s} \right] |P|^2, \quad P = \frac{C_{10}}{C_{10}^{\text{SM}}} \equiv |P|e^{i\varphi_P}, \quad (25)$$

where

$$\mathcal{A}_{\Delta\Gamma}^{\mu\mu} = \cos(2\varphi_P - 2\varphi_{B_s}), \quad y_s \equiv \tau_{B_s} \frac{\Delta\Gamma_s}{2} = 0.088 \pm 0.014. \quad (26)$$

The *bar* indicates that $\Delta\Gamma_s$ effects have been taken into account. In the SM and CMFV $\mathcal{A}_{\Delta\Gamma}^{\mu\mu} = 1$ but in the LHS it is slightly smaller and we take this effect into account. Generally as shown in [16] $\mathcal{A}_{\Delta\Gamma}^{\mu\mu}$ can serve to test NP models as it can be determined in time-dependent measurements [48, 49]. Of interest is also the CP asymmetry

$$S_{\mu\mu}^s = \sin(2\varphi_P - 2\varphi_{B_s}), \quad (27)$$

which has been studied in detail in [14, 16] in the context of Z' models.

In the case of $B_d \rightarrow \mu^+\mu^-$ decay the formulae given above apply with s replaced by d and $y_d \approx 0$. While C_{10}^{SM} remains unchanged, C_{10}^{NP} is clearly modified through the replacement of V_{ts} by V_{td} and different Z' coupling to quarks. But the muon coupling remains unchanged and this will allow a correlation between $B_s \rightarrow \mu^+\mu^-$ and

$B_d \rightarrow \mu^+\mu^-$ which will be investigated within LHS here for the first time. Explicit formulae for $B_d \rightarrow \mu^+\mu^-$ can be found in [14].

Concerning the status of the branching ratios for $B_{s,d} \rightarrow \mu^+\mu^-$ decays we have

$$\overline{\mathcal{B}}(B_s \rightarrow \mu^+\mu^-)_{\text{SM}} = (3.56 \pm 0.18) \cdot 10^{-9}, \quad \overline{\mathcal{B}}(B_s \rightarrow \mu^+\mu^-) = (2.9 \pm 0.7) \times 10^{-9}, \quad (28)$$

$$\mathcal{B}(B_d \rightarrow \mu^+\mu^-)_{\text{SM}} = (1.05 \pm 0.07) \times 10^{-10}, \quad \mathcal{B}(B_d \rightarrow \mu^+\mu^-) = (3.6_{-1.4}^{+1.6}) \times 10^{-10}, \quad (29)$$

where the SM values are based on [16, 50] and experimental data are the most recent average of the results from LHCb and CMS [28–30].

In the case of $B \rightarrow K^*\mu^+\mu^-$ we will concentrate our discussion on the Wilson coefficient C_9^{NP} which can be extracted from the angular observables, in particular $\langle F_L \rangle$, $\langle S_5 \rangle$ and $\langle A_8 \rangle$, in which within the LHS NP contributions enter exclusively through this coefficient. On the other hand $\text{Im}(C_{10}^{\text{NP}})$ governs the CP-asymmetry $\langle A_7 \rangle$. Useful approximate expressions for these four angular observables in terms of C_9^{NP} and C_{10}^{NP} have been provided in [26].

The recent $B \rightarrow K^*\mu^+\mu^-$ anomalies imply the following ranges for $C_9^{\text{NP}}(B_s)$ [26, 34] respectively

$$C_9^{\text{NP}}(B_s) = -(1.6 \pm 0.3), \quad C_9^{\text{NP}}(B_s) = -(0.8 \pm 0.3) \quad (30)$$

As $C_9^{\text{SM}}(B_s) \approx 4.1$ at $\mu_b = 4.8 \text{ GeV}$, these are very significant suppressions of this coefficient. We note that C_9 remains real as in the SM. We will have a closer look at the implications of this result for both values quoted above. The details behind these two results that differ by a factor of two is discussed in [26]. In fact inspecting Figs. 3 and 4 of the latter paper one sees that if the constraints from A_{FB} and $B \rightarrow K\mu^+\mu^-$ were not taken into account $C_9^{\text{NP}}(B_s) \approx -1.4$ could alone explain the anomalies in the observables F_L and S_5 . But the inclusion of these constraints reduces the size of this coefficient. Yet values of $C_9^{\text{NP}}(B_s) \approx -(1.2 - 1.0)$ seem to give reasonable agreement with all data and the slight reduction of departure of F_L and S_5 from their SM values in the future data would allow to explain the two anomalies with the help of $C_9^{\text{NP}}(B_s)$ as suggested originally in [34].

Further support for this picture comes from our analysis below and a very recent comprehensive Bayesian analysis of the authors of [51, 52] in [53], that appeared after our paper. They find that although SM works well, if one wants to interpret the data in extensions of the SM then NP scenarios with dominant NP effect in C_9 are favoured although the inclusion of chirality-flipped operators in agreement with [26] would help to reproduce the data. This is also confirmed in the very recent paper in [54]. References to earlier papers on $B \rightarrow K^*\mu^+\mu^-$ by all these authors can be found in [26, 34, 52] and [1].

2.4 Correlations between $\Delta M_{s,d}$, $B_{s,d} \rightarrow \mu^+\mu^-$ and C_9^{NP}

In [14] a number of correlations between $\Delta F = 2$ and $\Delta F = 1$ observables in LHS have been identified. Here we want to concentrate on the correlations between $\Delta M_{s,d}$,

$B_{s,d} \rightarrow \mu^+ \mu^-$ and C_9^{NP} as they can be exposed analytically.

First the CMFV relation between $\mathcal{B}(B_q \rightarrow \mu^+ \mu^-)$ and $\Delta M_{s,d}$ [25] generalizes in LHS to ($q = s, d$)

$$\mathcal{B}(B_q \rightarrow \mu^+ \mu^-) = C \frac{\tau_{B_q} |Y_A^q|^2}{\hat{B}_q |S(B_q)|} \Delta M_q, \quad (31)$$

$$\text{with } C = 6\pi \frac{\eta_Y^2}{\eta_B^2} \left(\frac{\alpha}{4\pi \sin^2 \theta_W} \right)^2 \frac{m_\mu^2}{M_W^2} = 4.395 \cdot 10^{-10}, \quad (32)$$

$S(B_q)$ given in (13) and

$$Y_A^q = \eta_Y Y_0(x_t) + \frac{\Delta_L^{qb}(Z') [\Delta_A^{\mu\bar{\mu}}(Z')]}{V_{tb} V_{tq}^* M_{Z'}^2 g_{\text{SM}}^2}. \quad (33)$$

Note that these relations are free from F_{B_q} dependence but in contrast to CMFV they depend on V_{tq} as generally $\Delta_L^{qb}(Z')$ are not aligned with $V_{tb} V_{tq}^*$. The main uncertainty in these relations comes from the parameters \hat{B}_q that are known presently with an accuracy of $\pm 8\%$ and $\pm 4.5\%$ for \hat{B}_d and \hat{B}_s , respectively (see new version of FLAG [55]). More accurate is the relation [25]

$$\frac{\mathcal{B}(B_s \rightarrow \mu^+ \mu^-)}{\mathcal{B}(B_d \rightarrow \mu^+ \mu^-)} = \frac{\hat{B}_d \tau(B_s) \Delta M_s}{\hat{B}_s \tau(B_d) \Delta M_d} r, \quad r = \left| \frac{Y_A^s}{Y_A^d} \right|^2 \left| \frac{S(B_d)}{S(B_s)} \right|, \quad \frac{\hat{B}_d}{\hat{B}_s} = 0.99 \pm 0.02 \quad (34)$$

where the departure of r from unity measures effects which go beyond CMFV. Still as shown already in [25] in the context of supersymmetric models with MFV and in the context of GMFV in [7] at large $\tan \beta$ one also finds $r \approx 1$ so that this relation offers also a test of these scenarios. On the other hand the most general test of MFV, as emphasized in [56], is the proportionality of the ratio of the two branching ratios in question to $|V_{ts}|^2/|V_{td}|^2$.

It should be noted that in (34) the only theoretical uncertainty enters through the ratio \hat{B}_s/\hat{B}_d that is already now known from lattice calculations with impressive accuracy of roughly $\pm 2\%$ [57] as given in (34)³. Therefore the relation (34) should allow a precision test of CMFV, related scenarios mentioned above and LHS even if the branching ratios $\mathcal{B}(B_{s,d} \rightarrow \mu^+ \mu^-)$ would turn out to deviate from SM predictions only by 10 – 15%. We should emphasize that such a precision test is not possible with any angular observable in $B_d \rightarrow K^* \mu^+ \mu^-$ due to form factor uncertainties. On the other hand these observables provide more information on NP than the relation (34).

In fact as seen in Fig. 9 the present data for r differ from its CMFV value ($r = 1$) by more than a factor of four

$$r_{\text{exp}} = 0.23 \pm 0.11. \quad (35)$$

³This result is not included in the recent FLAG update which quotes 0.95 ± 0.10 .

Even if in view of large experimental uncertainties one cannot claim that here NP is at work, this plot invites us to investigate whether LHS could cope with the future more precise experimental results in which the central values of the branching ratios in (28) and (29) would not change by much.

As far as the Wilson coefficients C_9^{NP} and C_{10}^{NP} are concerned we have two important relations

$$(\Delta S)^* = 4\tilde{r}g_{\text{SM}}^2 \sin^4 \theta_W \left[\frac{C_9^{\text{NP}}}{\bar{\Delta}_V^{\mu\bar{\mu}}(Z')} \right]^2 = 0.037 \left[\frac{C_9^{\text{NP}}}{\Delta_V^{\mu\bar{\mu}}(Z')} \right]^2 \left[\frac{M_{Z'}}{1 \text{ TeV}} \right]^2, \quad (36)$$

$$(\Delta S)^* = 4\tilde{r}g_{\text{SM}}^2 \sin^4 \theta_W \left[\frac{C_{10}^{\text{NP}}}{\bar{\Delta}_A^{\mu\bar{\mu}}(Z')} \right]^2 = 0.037 \left[\frac{C_{10}^{\text{NP}}}{\Delta_A^{\mu\bar{\mu}}(Z')} \right]^2 \left[\frac{M_{Z'}}{1 \text{ TeV}} \right]^2, \quad (37)$$

which we have written in a form suitable for the analysis in Section 6. We recall that $S_{\text{SM}} = S_0(x_t) = 2.31$.

These relations can be derived from (14), (22) and (23). The last relation, already encoded in previous relations, has been extensively studied in [14] for fixed value of the coupling $\bar{\Delta}_A^{\mu\bar{\mu}}(Z')$. It is evident that independently of the sign of this coupling in the case of a real C_{10}^{NP} , ΔS and ΔM_s will be enhanced which with the lattice value $\sqrt{\hat{B}_{B_s} F_{B_s}} = (279 \pm 13) \text{ MeV}$ [58] used in [14] would be a problem [59]. Making C_{10}^{NP} complex allowed through destructive interference with the SM contribution to lower the value of ΔM_s and bring it to agree with the data. With the new value for $\sqrt{\hat{B}_{B_s} F_{B_s}}$ MeV given below this problem is softened.

Concerning (36), we note that in the case of a real C_{10}^{NP} , the relation (24) implies that also C_9^{NP} must be real in LHS so that also this relation implies in this case uniquely an enhancement of ΔS and ΔM_s .

In the next section we will get an idea on the range of the values of $\bar{\Delta}_A^{\mu\bar{\mu}}(Z')$ by looking simultaneously at $B_s \rightarrow \mu^+ \mu^-$ and $B_d \rightarrow \mu^+ \mu^-$ decays. In the case of $\bar{\Delta}_V^{\mu\bar{\mu}}(Z')$ the simultaneous consideration of the decays $B_d \rightarrow K^* \mu^+ \mu^-$ and $B_d \rightarrow \rho \mu^+ \mu^-$ could give us in principle information about the size of this coupling. However, there is not enough experimental information on the latter decay and such an exercise cannot be performed at present.

On the other hand in the context of (36) it has been noted in [27] that $\bar{\Delta}_V^{\mu\bar{\mu}}(Z')$ could be eliminated in favour of the violation of the CKM unitarity in Z' models studied by Marciano and Sirlin long time ago [60] if one assumes that $\Delta_A^{sb} = 0$ and the diagonal couplings of Z' to quarks vanish. As already admitted by the authors of [27] such a model is not realistic. Therefore we provide here a more general formula which uses the results in [60] without making the assumptions made in [27].

We denote the violation of CKM unitarity by

$$\tilde{\Delta}_{\text{CKM}} = 1 - \sum_{q=d,s,b} |V_{uq}|^2 = -\Delta_{\text{CKM}}, \quad (38)$$

with Δ_{CKM} used in [27, 60]. Then for $M_{Z'} \gg M_W$ we find

$$\tilde{\Delta}_{\text{CKM}} = \frac{3\sqrt{2}}{8G_F} \frac{\alpha}{\pi \sin^2 \theta_W} \bar{\Delta}_L^{\mu\bar{\mu}}(Z') (\bar{\Delta}_L^{\mu\bar{\mu}}(Z') - \bar{\Delta}_L^{d\bar{d}}(Z')) \ln \frac{M_{Z'}^2}{M_W^2}, \quad (39)$$

where $\bar{\Delta}_L^{d\bar{d}}$ is the diagonal coupling of Z' to down-quarks which is assumed to be generation independent.

The triple correlation between ΔM_s , $\tilde{\Delta}_{\text{CKM}}$ and C_9^{NP} found in [27] only follows for the case

$$\bar{\Delta}_V^{\mu\bar{\mu}}(Z') = \frac{\bar{\Delta}_L^{\mu\bar{\mu}}(Z')}{2}, \quad \bar{\Delta}_L^{d\bar{d}}(Z') = 0, \quad (40)$$

where the first equality is equivalent to $\bar{\Delta}_A^{\mu\bar{\mu}}(Z') = 0$. The triple correlation in question can now be rewritten as

$$(\Delta S)^* \tilde{\Delta}_{\text{CKM}} = \frac{3}{4} \tilde{r} \left(\frac{\alpha}{\pi}\right)^2 (C_9^{\text{NP}})^2 \ln \frac{M_{Z'}^2}{M_W^2}, \quad (41)$$

which allows better to follow the signs than the expression given by these authors. As now $\tilde{\Delta}_{\text{CKM}} \geq 0$, it is evident also from this formula that in the case of a real C_9^{NP} , independently of its sign, ΔS is real and strictly positive enhancing uniquely ΔM_s . In [27] only $|\Delta S|$ has been studied.

However, generally the assumptions in (40) are violated and in examples shown in [60] there is always a quark contribution to $\tilde{\Delta}_{\text{CKM}}$. In fact these authors present GUT examples where the quark contribution cancels the one of leptons so that in such a model there is no violation of CKM unitarity.

Independently of this discussion the case of a real C_9^{NP} is interesting in itself and in Section 6 we will investigate how the predictions of the LHS model would look like in the presence of a real C_9^{NP} as large as required to remove the anomalies in the data on $B_d \rightarrow K^* \mu^+ \mu^-$.

3 Determining the parameters in the LHS

In principle there are many ways to bound or even determine the reduced parameters in (1). Here we present one route which simultaneously allows already at the early stage to test the LHS. This route could be improved and modified dependently on evolution of experimental data.

To this end we use the parametrization

$$\bar{\Delta}_L^{sb}(Z') = -|\bar{\Delta}_L^{sb}(Z')| e^{i\delta_{23}}, \quad |\bar{\Delta}_L^{sb}(Z')| = \frac{\tilde{s}_{23}}{M_{Z'}}, \quad (42)$$

where \tilde{s}_{23} and δ_{23} are parameters used in [14] and the minus sign is introduced to cancel the minus sign in V_{ts} in the relevant phenomenological formulae. For $B_d - \bar{B}_d^0$ mixing and $B_d \rightarrow \mu^+ \mu^-$ s is replaced by d and no minus sign is introduced. Moreover δ_{23} is replaced by δ_{13} .

Step 1

Measurements of ΔM_s , $S_{\psi\phi}$ and $\Delta\Gamma_s$ determine uniquely $|\bar{\Delta}_L^{sb}(Z')|$ and two values of the phase δ_{23} , differing by 180° corresponding to two oases determined in [14]: *blue* and *purple* oasis for low and high δ_{23} , respectively. Equivalently the phase δ_{23} could be fixed through the blue oasis. The purple oasis is then reached by just flipping the sign of $\bar{\Delta}_L^{sb}(Z')$.

The same procedure is applied to the B_d -system which determines $\bar{\Delta}_L^{db}(Z')$. The two values for the phase δ_{13} correspond to *yellow* and *green* oasis in [14], respectively. It should be recalled that the outcome of this determination depends on the value of $|V_{ub}|$ resulting in two LHS scenarios, LHS1 and LHS2, corresponding to exclusive and inclusive determinations of $|V_{ub}|$. This point is elaborated at length in [1, 14].

Step 2

With the result of Step 1 we can immediately perform an important test of the LHS as in this model in the $b \rightarrow s\mu^+\mu^-$ case

$$\frac{\text{Im}(C_9^{\text{NP}})}{\text{Re}(C_9^{\text{NP}})} = \frac{\text{Im}(C_{10}^{\text{NP}})}{\text{Re}(C_{10}^{\text{NP}})} = \tan(\delta_{23} - \beta_s). \quad (43)$$

Two important points should be noticed here. These two ratios have to be equal to each other. Moreover they do not depend on whether we are in the blue or purple oasis. This test is interesting in the context of recent proposals that C_9^{NP} could be real. We point out that in the context of LHS this proposal can be tested through the correlation with $B_s^0 - \bar{B}_s^0$ mixing. We will elaborate on it in Section 6.

Step 3

In order to determine $|\bar{\Delta}_A^{\mu\bar{\mu}}(Z')|$ we use $\bar{\mathcal{B}}(B_s \rightarrow \mu^+\mu^-)$ together with results of Step 1. The sign of this coupling cannot be determined uniquely as only the product of the couplings $\bar{\Delta}_L^{sb}(Z')$ and $\bar{\Delta}_A^{\mu\bar{\mu}}(Z')$ is measured by $\bar{\mathcal{B}}(B_s \rightarrow \mu^+\mu^-)$. As the sign of $\bar{\Delta}_L^{sb}(Z')$ could not be fixed in Step 1 also the sign of $\bar{\Delta}_A^{\mu\bar{\mu}}(Z')$ cannot be determined. Yet this ambiguity has no impact on physical implications as the measurements of ΔM_s , $S_{\psi\phi}$ and $\bar{\mathcal{B}}(B_s \rightarrow \mu^+\mu^-)$ correlate the signs of these two couplings so that once the three observables have been measured it is irrelevant whether the subsequent calculations are performed in the blue or purple oasis. Moving from one oasis to the other will require simultaneous change of the sign of $\bar{\Delta}_A^{\mu\bar{\mu}}(Z')$ to agree with the data on $\bar{\mathcal{B}}(B_s \rightarrow \mu^+\mu^-)$. The subsequent predictions for $S_{\mu\mu}^s$ and $\langle A_7 \rangle$ and the correlations of these two observables with ΔM_s , $\bar{\mathcal{B}}(B_s \rightarrow \mu^+\mu^-)$ and $S_{\psi\phi}$ will not be modified in the new oasis.

However when the result for $|\bar{\Delta}_A^{\mu\bar{\mu}}(Z')|$ determined in this manner is used in conjunction with $\bar{\Delta}_L^{db}(Z')$ obtained in Step 1 to predict $\mathcal{B}(B_d \rightarrow \mu^+\mu^-)$ the final result will depend

on the sign of these two couplings. But this difference will be distinguished simply through the enhancement or suppression of this branching ratio relative to its SM value. Moreover the value of $\mathcal{B}(B_d \rightarrow \mu^+ \mu^-)$ will depend on whether LHS1 or LHS2 is considered.

Step 4

In order to determine $|\bar{\Delta}_V^{\mu\bar{\mu}}(Z')|$ we have to know C_9^{NP} which can be extracted from one of the following angular observables: $\langle F_L \rangle$, $\langle S_5 \rangle$ and $\langle A_8 \rangle$. Again only the product of $\bar{\Delta}_L^{sb}(Z')$ and $\bar{\Delta}_V^{\mu\bar{\mu}}(Z')$ is determined in this manner and consequently the sign of $\bar{\Delta}_V^{\mu\bar{\mu}}(Z')$ cannot be determined uniquely as was the case of $\bar{\Delta}_A^{\mu\bar{\mu}}(Z')$ in Step 3. Yet, one can convince oneself that the correlations between these three observables and the ones in the B_s meson system considered in previous steps, do not depend on this sign once the products of couplings in questions have been determined uniquely in Step 3 and this step.

Step 5

As the determination of quark and muon couplings is completed we can first determine $\bar{\Delta}_L^{\nu\bar{\nu}}(Z')$ by means of (2) and subsequently make unique predictions for all $b \rightarrow s\nu\bar{\nu}$ transitions. Indeed in this case the relevant one-loop function is

$$X_L(B_s) = \eta_X X_0(x_t) + \left[\frac{\bar{\Delta}_L^{\nu\nu}(Z')}{g_{\text{SM}}^2} \right] \frac{\bar{\Delta}_L^{sb}(Z')}{V_{ts}^* V_{tb}} \equiv \eta_X X_0(x_t) + C_{\nu\bar{\nu}}^{\text{NP}}, \quad (44)$$

where the first term is the SM contribution given in [14]. Using the relevant formulae in [61], unique predictions, independent of the sign of $\bar{\Delta}_L^{\nu\bar{\nu}}(Z')$, for $B_d \rightarrow K\nu\bar{\nu}$, $B_d \rightarrow K^*\nu\bar{\nu}$ and $B_d \rightarrow X_s\nu\bar{\nu}$ can be made. Indeed we obtain by means of (2) an important relation

$$C_{\nu\bar{\nu}}^{\text{NP}} = \sin^2 \theta_W \frac{C_{10}^{\text{NP}} - C_9^{\text{NP}}}{2}. \quad (45)$$

4 Correlations between flavour observables in the LHS

4.1 Preliminaries

Having all these results at hand we want to illustrate this procedure and the implied correlations numerically. As already pointed out and analyzed in detail in [14] due the strong correlations between $\Delta F = 2$ and $\Delta F = 1$ observables within LHS, the pattern and size of allowed NP effects in the latter observables depends crucially on

the room left for NP contributions in $\Delta F = 2$ observables. Therefore we briefly review the situation in $B_{s,d} - \bar{B}_{s,d}$ mixings. In contrast to CMFV models we do not have to discuss simultaneously the ΔM_K and ε_K as generally there is no correlation of these observables with $B_{s,d} - \bar{B}_{s,d}$ mixings. This allows to avoid certain tension in CMFV models analysed recently by us [59].

It is useful to recall the parametric dependence of $\Delta M_{s,d}$ within the SM. One has⁴

$$(\Delta M_s)_{\text{SM}} = 17.7/\text{ps} \cdot \left[\frac{\sqrt{\hat{B}_{B_s}} F_{B_s}}{267 \text{ MeV}} \right]^2 \left[\frac{S_0(x_t)}{2.31} \right] \left[\frac{|V_{ts}|}{0.0402} \right]^2 \left[\frac{\eta_B}{0.55} \right], \quad (46)$$

$$(\Delta M_d)_{\text{SM}} = 0.51/\text{ps} \cdot \left[\frac{\sqrt{\hat{B}_{B_d}} F_{B_d}}{218 \text{ MeV}} \right]^2 \left[\frac{S_0(x_t)}{2.31} \right] \left[\frac{|V_{td}|}{8.5 \cdot 10^{-3}} \right]^2 \left[\frac{\eta_B}{0.55} \right] \quad (47)$$

We observe that for the chosen central values of the parameters there is a perfect agreement with the very accurate data [62]:

$$\Delta M_s = 17.69(8) \text{ ps}^{-1}, \quad \Delta M_d = 0.510(4) \text{ ps}^{-1}. \quad (48)$$

In fact these central values are very close to the central values presented recently by the Twisted Mass Collaboration [57]

$$\sqrt{\hat{B}_{B_s}} F_{B_s} = 262(10) \text{ MeV}, \quad \sqrt{\hat{B}_{B_d}} F_{B_d} = 216(10) \text{ MeV}. \quad (49)$$

Similar values 266(18) MeV and 216(15) with larger errors are quoted by FLAG, where the new results in (49) are not yet included. While the central values in (49) are lower than the ones used by us in [14] they agree with the latter within the errors, in particular when the numbers from FLAG are considered.

Concerning $S_{\psi\phi}$ and $S_{\psi K_S}$ we have

$$S_{\psi\phi} = - (0.04_{-0.13}^{+0.10}), \quad S_{\psi K_S} = 0.679(20) \quad (50)$$

with the second value known already for some time [62] and the first one being the most recent average from HFAG [62] close to the earlier result from the LHCb [63]. The first value is consistent with the SM expectation of 0.04. This is also the case of $S_{\psi K_S}$ but only for exclusive determination of $|V_{ub}| \approx (3.4 \pm 0.2) \times 10^{-3}$ [1]. When the inclusive determination of $|V_{ub}|$, like $(4.2 \pm 0.2) \times 10^{-3}$, is used $S_{\psi K_S}$ is found above 0.77 and NP is required to bring it down to its experimental value with interesting implications for $\Delta F = 1$ observables as shown in [14] and below.

⁴The central value of $|V_{ts}|$ corresponds roughly to the central $|V_{cb}| = 0.0409$ obtained from tree-level decays.

While there is some feeling in the community that there is no NP in $S_{\psi\phi}$ we would like to stress again [1] that a precise measurement of this observable is very important as it provides powerful tests of various NP scenarios. In particular the distinction between CMFV models based on $U(3)^3$ flavour symmetry and $U(2)^3$ models can be performed by studying triple correlation $S_{\psi\phi} - S_{\psi K_S} - |V_{ub}|$ [11]. We will also see below that this determination is also important for the tests of the LHS model through the observables considered here.

4.2 Strategy

It is to be expected that in flavour precision era, which will include both advances in experiment and theory, in particular lattice calculations, it will be possible to decide with high precision whether ΔM_s and ΔM_d within the SM agree or disagree with the data. For instance already the need for enhancements or suppressions of these observables would be an important information. Similar comments apply to $S_{\psi\phi}$ and $S_{\psi K_S}$ as well as to the branching ratios $\mathcal{B}(B_{s,d} \rightarrow \mu^+ \mu^-)$. In particular the correlations and anti-correlations between the suppressions and enhancements allow to distinguish between various NP models as can be illustrated with the DNA charts proposed in [1].

In order to monitor this progress in the context of the LHS model we use the ratios [64]:

$$C_{B_s} = \frac{\Delta M_s}{(\Delta M_s)_{\text{SM}}} = \frac{|S(B_s)|}{S_0(x_t)}, \quad C_{B_d} = \frac{\Delta M_d}{(\Delta M_d)_{\text{SM}}} = \frac{|S(B_d)|}{S_0(x_t)} \quad (51)$$

that in the LHS, thanks to the presence of a single operator do not involve any non-perturbative uncertainties. Of course in order to find out the experimental values of these ratios one has to handle these uncertainties but this is precisely what we want to monitor in the coming years. The most recent update from Ufit collaboration reads

$$C_{B_s} = 1.08 \pm 0.09, \quad C_{B_d} = 1.10 \pm 0.17 . \quad (52)$$

4.3 Performing steps 1 and 2

Using this strategy we can perform Step 1. In Fig. 1 we show in the case of the $B_s^0 - \bar{B}_s^0$ system $|\bar{\Delta}_L^{sb}(Z')|$ and the phase δ_{23} as functions of C_{B_s} for different values of $S_{\psi\phi}$. The results are given for the blue oasis (low δ_{23}). For the purple oasis (high δ_{23}) one just has to add 180° to δ_{23} . In Fig. 2 we repeat this exercise for the $B_d^0 - \bar{B}_d^0$ system setting $\beta = 21.2^\circ$ extracted using the exclusive value of $|V_{ub}| = 3.4 \times 10^{-3}$. This corresponds to the LHS1 scenario of [14]. In Fig. 3 we show the results for LHS2 scenario with $\beta = 25.2^\circ$ corresponding to $|V_{ub}| = 4.0 \times 10^{-3}$ and in the ballpark of inclusive determinations of this CKM element.

Our colour coding for the values of $S_{\psi\phi}$ and $S_{\psi K_S}$ is as follows:

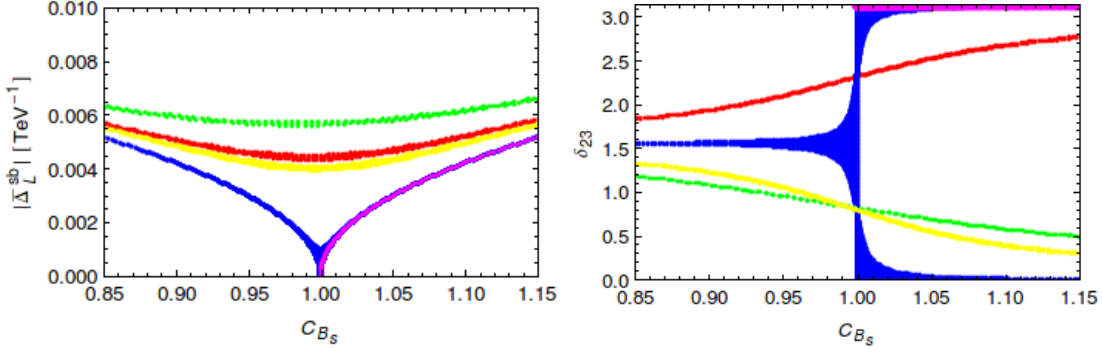


Figure 1: $|\bar{\Delta}_L^{sb}|$ and δ_{23} versus $C_{B_s} = \Delta M_s / \Delta M_s^{\text{SM}}$ for $S_{\psi\phi} \in [0.14, 0.15]$ (red), $[0.03, 0.04]$ (blue), $[-0.06, -0.05]$ (yellow) and $[-0.15, -0.14]$ (green). The magenta line is for real C_9^{NP} , i.e. for $\delta_{23} = \beta_s(+\pi)$.

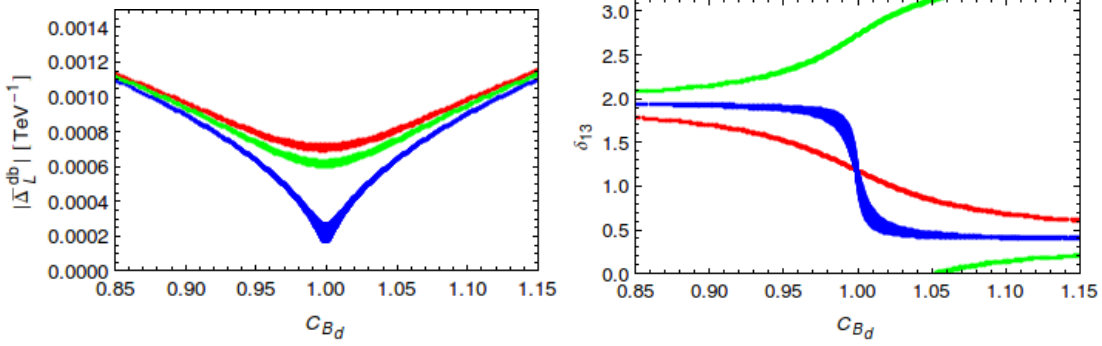


Figure 2: $|\bar{\Delta}_L^{db}|$ and δ_{13} versus $C_{B_d} = \Delta M_d / \Delta M_d^{\text{SM}}$ for $|V_{ub}| = 0.0034$ and $S_{\psi K_S} \in [0.718, 0.722]$ (red), $[0.678, 0.682]$ (blue), $[0.638, 0.642]$ (green).

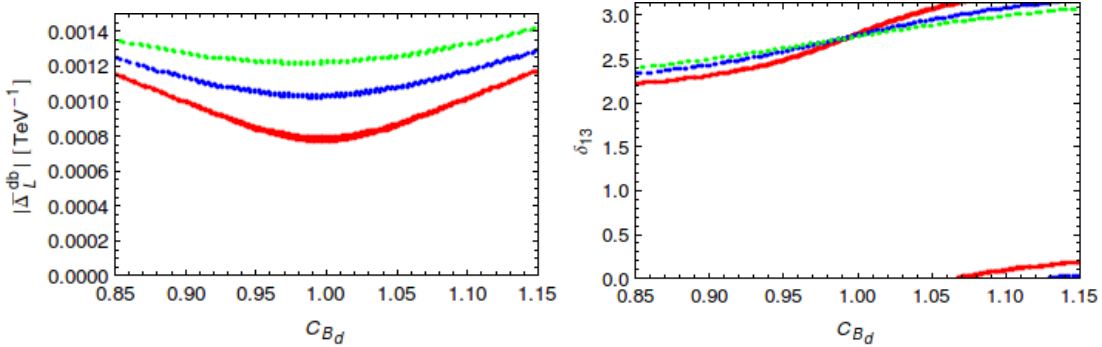


Figure 3: $|\bar{\Delta}_L^{db}|$ and δ_{13} versus $C_{B_d} = \Delta M_d / \Delta M_d^{\text{SM}}$ for $|V_{ub}| = 0.0040$ and $S_{\psi K_S} \in [0.718, 0.722]$ (red), $[0.678, 0.682]$ (blue), $[0.638, 0.642]$ (green).

- In the case of $B_s^0 - \bar{B}_s^0$ we fix $S_{\psi\phi}$ to the following ranges: *red* (0.14 – 0.15), *blue* (0.03 – 0.04), *yellow* (–(0.05 – 0.06)), *green* (–(0.14 – 0.15)).

- In the case of $B_d^0 - \bar{B}_d^0$ we fix $S_{\psi K_S}$ to the following ranges: *red* (0.718 – 0.722), *blue* (0.678 – 0.682), *green* (0.638 – 0.642).

The following observations can be made on the basis of these plots.

- The value of $|\bar{\Delta}_L^{sb}(Z')|$ vanishes in the blue scenario when $C_{B_s} = 1$ as in this scenario also $S_{\psi\phi}$ is very close to its SM value. In other scenarios for $S_{\psi\phi}$ the coupling $|\bar{\Delta}_L^{sb}(Z')|$ is non-vanishing even for $C_{B_s} = 1$ as LHS has to bring $S_{\psi\phi}$ to agree with data. The more the value of $S_{\psi\phi}$ differs from the SM one, the larger $|\bar{\Delta}_L^{sb}(Z')|$ is allowed to be. Its value increases with increasing $|C_{B_s} - 1|$ and this increase is strongest in the blue scenario.
- The value of δ_{23} in the blue scenario is arbitrary for $C_{B_s} = 1$ but as in this case $|\bar{\Delta}_L^{sb}(Z')|$ vanishes NP contributions vanish anyway. In this scenario for $C_{B_s} < 1$ we find $\delta_{23} \approx \pi/2$. For $C_{B_s} > 1$ one has $\delta_{23} \approx (0, \pi)$. In the red scenario, in which $S_{\psi\phi}$ is larger than its SM value δ_{23} is confined to the second quadrant and increases monotonically with increasing C_{B_s} . In the yellow and green scenario in which $S_{\psi\phi}$ is negative, δ_{23} is confined to the first quadrant and decreases monotonically with increasing C_{B_s} .
- We note that in red, yellow and green scenarios for $S_{\psi\phi}$, in the full range of C_{B_s} considered, δ_{23} has to differ from 0, $\pi/2$ or π . Through (43) this implies that the coefficients C_9^{NP} and C_{10}^{NP} cannot be real. We show this in Fig. 4 for these three scenarios of $S_{\psi\phi}$. We observe that for green and yellow scenarios for which $S_{\psi\phi} < 0$, the ratio in question is positive, while it is negative for $S_{\psi\phi}$ larger than the SM value. Moreover for C_{B_s} significantly smaller than unity, where large NP phase is required to obtain correct value for ΔM_s the ratios in (43) have to be large. This is not the case for $C_{B_s} > 1$ as then a real C_9^{NP} implies automatically an enhancement of C_{B_s} as we will discuss in Section 6.
- Turning now our discussion to the $B_d^0 - \bar{B}_d^0$ system we observe that in the LHS1 scenario δ_{13} is confined to the first quadrant in the red scenario where $S_{\psi K_S}$ is larger than its SM value and dominantly in the second quadrant (green scenario) when it is below it. In the LHS2 scenario $|\bar{\Delta}_L^{db}(Z')|$ is always different from zero as the SM value of $S_{\psi K_S}$ being in our example 0.77 is larger than its experimental value in red, blue and green scenarios considered and NP has to remove this discrepancy.

In summary once $S_{\psi\phi}$, C_{B_s} , $S_{\psi K_S}$ and C_{B_d} are precisely known plots in Figs. 1-3 will allow to obtain precise values of $|\bar{\Delta}_L^{sb}(Z')|$, δ_{23} , $|\bar{\Delta}_L^{db}(Z')|$, δ_{13} allowing the predictions for other observables.

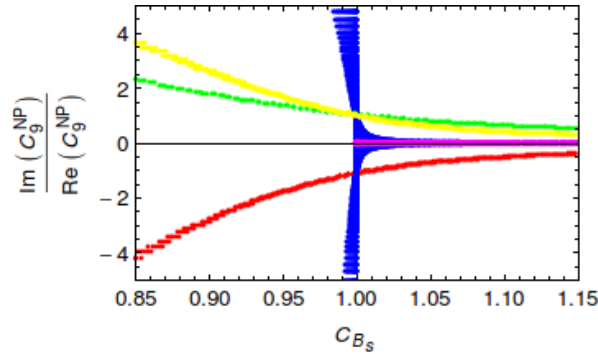


Figure 4: $\text{Im}(C_9^{\text{NP}})/\text{Re}(C_9^{\text{NP}}) = \text{Im}(C_{10}^{\text{NP}})/\text{Re}(C_{10}^{\text{NP}})$ versus $C_{B_s} = \Delta M_s/\Delta M_s^{\text{SM}}$ for $S_{\psi\phi} \in [0.14, 0.15]$ (red), $[0.03, 0.04]$ (blue), $[-0.06, -0.05]$ (yellow) and $[-0.15, -0.14]$ (green). The magenta line is for real C_9^{NP} , i.e. for $\delta_{23} = \beta_s(+\pi)$.

4.4 Performing step 3

In [14] we have set $\bar{\Delta}_A^{\mu\bar{\mu}}(Z') = 0.5/\text{TeV}$. The goal of this step is to determine which values of this coupling are consistent with the present values of the branching ratios for $B_{s,d} \rightarrow \mu^+\mu^-$ decays. The status of these branching ratios has been summarized in (28) and (29).

In order to get an idea what values of $\bar{\Delta}_A^{\mu\bar{\mu}}(Z')$ are consistent with these data and with the data on CP-asymmetries $S_{\psi\phi}$ and $S_{\psi K_S}$, we study the correlations between $\bar{\mathcal{B}}(B_s \rightarrow \mu^+\mu^-)$ and $S_{\psi\phi}$ and between $\mathcal{B}(B_d \rightarrow \mu^+\mu^-)$ and $S_{\psi K_S}$ for four different values of $|\bar{\Delta}_A^{\mu\bar{\mu}}(Z')|$ in five bins for C_{B_s} and C_{B_d} all to be listed below. This time in order to have a comparison with [14] we present the results for two oases: low and high δ_{23} for $B_s \rightarrow \mu^+\mu^-$ and low and high δ_{13} for $B_d \rightarrow \mu^+\mu^-$. Yet in order not to complicate colour coding we use the same colours for the two oases. The main difference with respect to [14] is the study of the dependence on $|\bar{\Delta}_A^{\mu\bar{\mu}}(Z')|$ and the consideration of values of $C_{B_{s,d}}$ smaller and larger than unity, whereas in that paper only $C_{B_{s,d}} < 1.0$ have been considered due to previous lattice results as discussed above. Moreover, anticipating progress in lattice calculations we consider several bins in $C_{B_{s,d}}$.

It turns out that the results for the correlations of $\bar{\mathcal{B}}(B_s \rightarrow \mu^+\mu^-)$ and $S_{\psi\phi}$ look rather involved and in order to increase the transparency of our presentation we have in this case shown two figures. In Fig. 5 we show five plots each corresponding to different bin in C_{B_s} and in each plot different colours correspond to different values of $\bar{\Delta}_A^{\mu\bar{\mu}}(Z')$. On the other hand in Fig. 6 we show four plots corresponding to different values of $\bar{\Delta}_A^{\mu\bar{\mu}}(Z')$ and in each plot different colours correspond to different values of C_{B_s} . The latter presentation turns out to be unnecessary in the case of the correlation $\mathcal{B}(B_d \rightarrow \mu^+\mu^-)$ and $S_{\psi K_S}$ for which the results are presented in Figs. 7 and 8 for the B_d system in LHS1 and LHS2 scenarios for $|V_{ub}|$, respectively.

The colour coding for $\bar{\Delta}_A^{\mu\bar{\mu}}(Z')$ in both B_s and B_d systems is

$$\bar{\Delta}_A^{\mu\bar{\mu}}(Z') = 0.50/\text{TeV (blue)}, \quad 1.00/\text{TeV (red)}, \quad 1.50/\text{TeV (green)}, \quad 2.00/\text{TeV (yellow)}. \quad (53)$$

Working with two oases it is sufficient to consider only positive values of $\bar{\Delta}_A^{\mu\bar{\mu}}(Z')$ as discussed above.

On the other hand the colour coding for C_{B_s} relevant only for Fig. 6 is as follows

$$C_{B_s} = 0.90 \pm 0.01 \text{ (blue)}, \quad 0.96 \pm 0.01 \text{ (green)}, \quad 1.00 \pm 0.01 \text{ (red)}, \quad (54)$$

$$C_{B_s} = 1.04 \pm 0.01 \text{ (cyan)}, \quad 1.10 \pm 0.01 \text{ (yellow)}$$

and similarly for C_{B_d} . Furthermore we include bounds for C_{10}^{NP} derived from $b \rightarrow s\ell\ell$ transitions [22, 65, 66]. As in [1] we use the following range

$$-0.8 \leq \text{Re}(C_{10}^{\text{NP}}) \leq 1.8, \quad -3 \leq \text{Im}(C_{10}) \leq 3. \quad (55)$$

The exact bounds are even smaller than these rectangular bounds. Clearly these bounds will be changing with time together with the modification of data but we show their impact here to illustrate how looking simultaneously at various observables can constrain a given NP scenario.

The main results of this exercise are as follows.

- In the case of the B_s system the correlation between $\bar{\mathcal{B}}(B_s \rightarrow \mu^+\mu^-)$ and $S_{\psi\phi}$ and the allowed values of $\bar{\Delta}_A^{\mu\bar{\mu}}(Z')$ depend strongly on the chosen value of C_{B_s} . Moreover, the constraints in (55), that eliminate the regions in black, have an important impact on these plots. The larger C_{B_s} , the more points are eliminated. For the last bin $C_{B_s} = 1.10 \pm 0.01$ the only points that survive are the ones with $\bar{\Delta}_A^{\mu\bar{\mu}} = 0.50/\text{TeV}$ and $\bar{\mathcal{B}}(B_s \rightarrow \mu^+\mu^-) \leq 1.7 \cdot 10^{-9}$ so that this bin is excluded. This can be seen in Fig. 6 and therefore we do not show this bin in Fig. 5
- As seen in Fig. 6 for $C_{B_s} = 0.96 \pm 0.01$ (green) basically all values of $\bar{\Delta}_A^{\mu\bar{\mu}}(Z')$ in (53) are allowed but this is no longer the case for other bins of C_{B_s} . In particular for $C_{B_s} \approx 0.90$ (blue) as considered in [14] the values $\bar{\Delta}_A^{\mu\bar{\mu}}(Z') \leq 1.0$ are favoured. In this case not only present data on $\bar{\mathcal{B}}(B_s \rightarrow \mu^+\mu^-)$ and $S_{\psi\phi}$ can be reproduced but also values close to SM expectations for these two observables are allowed.
- On the other hand for $C_{B_s} = 1.04$ (cyan) only $\bar{\Delta}_A^{\mu\bar{\mu}}(Z') \approx 0.5$ is allowed by all constraints and $\bar{\mathcal{B}}(B_s \rightarrow \mu^+\mu^-) \leq 2.5 \cdot 10^{-9}$ or around $5 \cdot 10^{-9}$. That is for this value of $C_{B_s} = 1.04$ the branching ratio in question differs sizably from the SM predictions and in fact $\bar{\Delta}_A^{\mu\bar{\mu}}(Z') < 0.5$ would give a better agreement with the data. But as we discuss below one needs $\bar{\Delta}_A^{\mu\bar{\mu}}(Z') \geq 1.0$ to obtain the agreement with the data for $\mathcal{B}(B_d \rightarrow \mu^+\mu^-)$. We conclude therefore that the present data on $B_{s,d} \rightarrow \mu^+\mu^-$ when the constraints in (55) are taken into account favour $C_{B_s} \leq 1.0$. Thus $\bar{\Delta}_A^{\mu\bar{\mu}}(Z') = 1.0$ and $C_{B_s} = 1.00 \pm 0.01$ appears to us to be the optimal combination when also $B_d \rightarrow \mu^+\mu^-$ is considered.

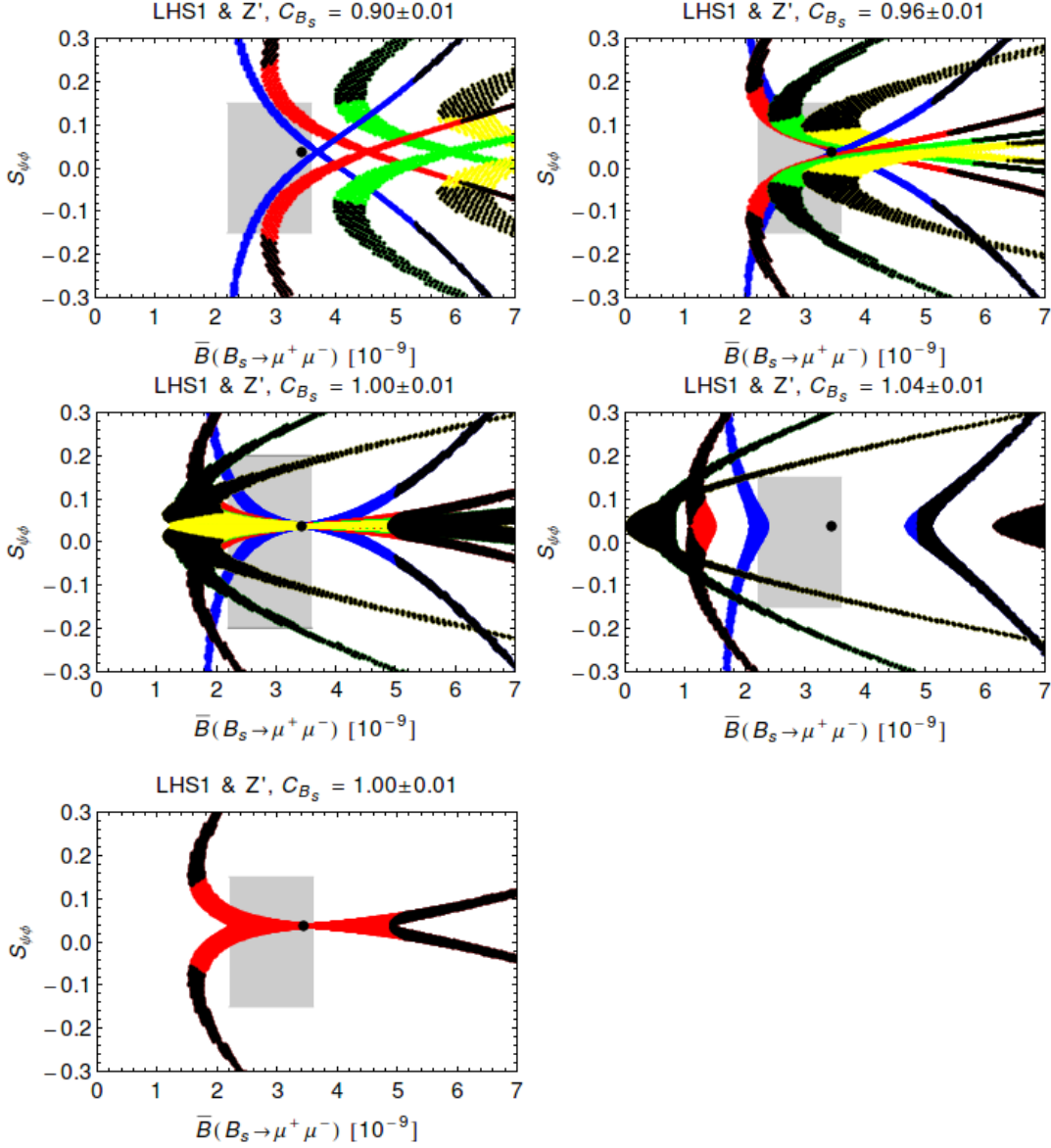


Figure 5: $S_{\psi\phi}$ versus $\bar{\mathcal{B}}(B_s \rightarrow \mu^+\mu^-)$ for different values of C_{B_s} (see Eq. (54)) and $\bar{\Delta}_A^{\mu\mu}$ (see Eq. (53)). In the last plot only $\bar{\Delta}_A^{\mu\mu} = 1 \text{ TeV}^{-1}$ for $C_{B_s} = 1.00 \pm 0.01$ is shown. The black regions violate the bounds for C_{10}^{NP} (see Eq. (55)). Black point: SM central value. The gray region represents the data.

- Indeed moving next to the B_d system we observe that basically only for $\bar{\Delta}_A^{\mu\mu}(Z') \geq 1.0$ can one reproduce the data for $\mathcal{B}(B_d \rightarrow \mu^+\mu^-)$ within 1σ . Moreover, it is striking that measuring this branching ratio and $S_{\psi K_S}$ precisely it is much easier to determine the coupling $\bar{\Delta}_A^{\mu\mu}(Z')$ than through the B_s system. This is of course the consequence of the large NP contribution needed to come close to the central

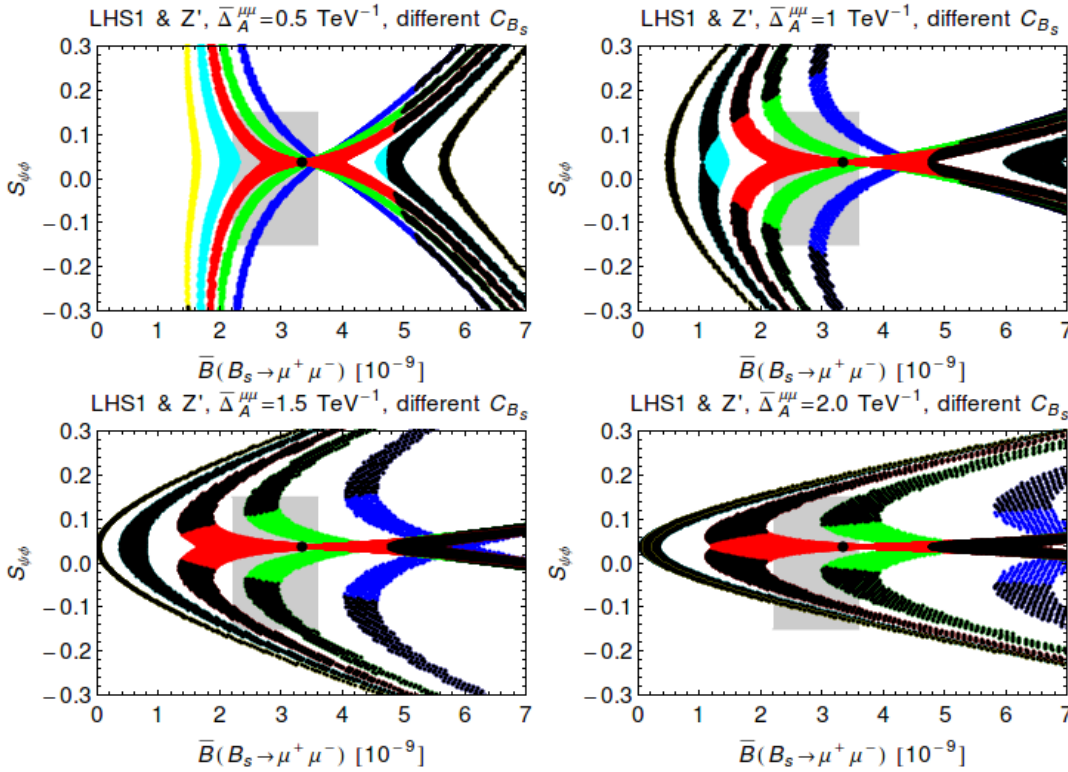


Figure 6: $S_{\psi\phi}$ versus $\bar{\mathcal{B}}(B_s \rightarrow \mu^+ \mu^-)$ for different values of C_{B_s} (see Eq. (54)) and fixed $\bar{\Delta}_A^{\mu\mu}$ (see caption of the plot). The black regions violate the bounds for C_{10}^{NP} (see Eq. (55)). Black point: SM central value. The gray region represents the data.

values of the CMS and LHCb data. We also observe that NP effects are larger in LHS2 scenario as in this case there is a bigger room for NP in $S_{\psi K_s}$ which has to be suppressed to agree with the data.

- We observe that if one does not want to work with values of $\bar{\Delta}_A^{\mu\mu}(Z')$ as high as 1.5/TeV and 2.0/TeV the data on $B_d \rightarrow \mu^+ \mu^-$ favour $C_{B_d} \geq 1.00$ and LHS2 scenario, although for $C_{B_d} \geq 1.04$ and $\bar{\Delta}_A^{\mu\mu}(Z') = 1.0/\text{TeV}$ also interesting results in LHS1 are obtained.

To summarize, the present data allow to find certain pattern in the couplings:

- The B_s system favours $C_{B_s} \leq 1.00$, while the B_d -system $C_{B_d} \geq 1.00$. Yet these two values cannot differ by more than 5% in order to reproduce the experimental ratio $\Delta M_s/\Delta M_d$ which contains smaller hadronic uncertainties than ΔM_s and ΔM_d separately.
- It appears that $\bar{\Delta}_A^{\mu\mu}(Z') \approx 1.0/\text{TeV}$ is the present favoured value for this coupling but it will go down if the unexpectedly large values of $\mathcal{B}(B_d \rightarrow \mu^+ \mu^-)$ will decrease in the future.

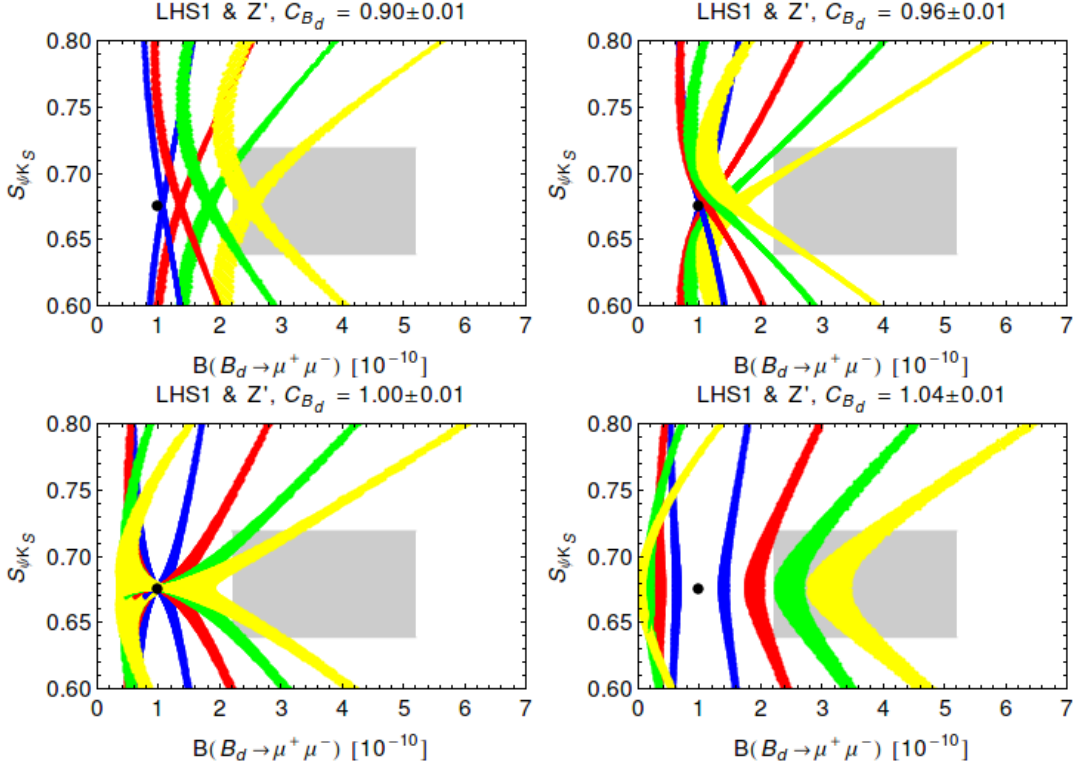


Figure 7: $S_{\psi K_S}$ versus $\mathcal{B}(B_d \rightarrow \mu^+ \mu^-)$ for $|V_{ub}| = 0.0034$ and different values of C_{B_d} (see Eq. (54)) and $\bar{\Delta}_A^{\mu\bar{\mu}}$ (see Eq. (53)). Black point: SM central value. The gray region represents the data.

With this information at hand let us see what impact these results have on the correlation between the two branching ratios in question. As Figs. 5-8 allow to find out what is the outcome of this exercise we only show two examples by setting

$$C_{B_s} = 1.00 \pm 0.01, \quad C_{B_d} = 1.04 \pm 0.01, \quad \bar{\Delta}_A^{\mu\bar{\mu}}(Z') = 1.0/\text{TeV} \quad (56)$$

and calculating $\mathcal{B}(B_d \rightarrow \mu^+ \mu^-)$ for the cases of LHS1 and LHS2. We varied the CP-asymmetries in the following ranges

$$-0.15 \leq S_{\psi\phi} \leq 0.15, \quad 0.639 \leq S_{\psi K_S} \leq 0.719. \quad (57)$$

The result is shown in Fig. 9 where the blue line corresponds to $r = 1$ in (34). For both LHS1 and LHS2 there are two regions corresponding to enhanced and suppressed values of $\mathcal{B}(B_d \rightarrow \mu^+ \mu^-)$. In the LHS2 case one finds that these two regions correspond to two different oases. Similar structure specific to the $C_{B_d} > 1$ region and LHS2 has been found in the context of the analysis of 331 models in [13] (see Fig. 20 of that paper). The origin of this behaviour is explained in detail in that paper with large values of $\mathcal{B}(B_d \rightarrow \mu^+ \mu^-)$ corresponding to larger phase δ_{13} for a chosen positive sign of $\bar{\Delta}_A^{\mu\bar{\mu}}(Z')$.

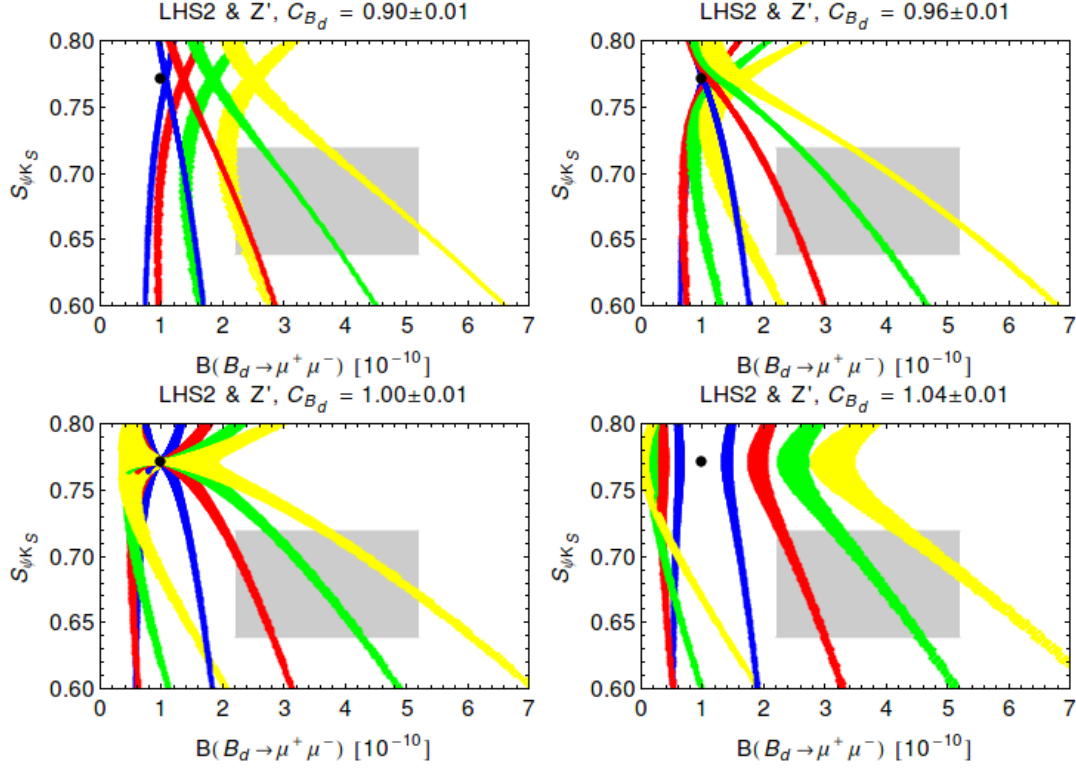


Figure 8: $S_{\psi K_S}$ versus $\mathcal{B}(B_d \rightarrow \mu^+ \mu^-)$ for $|V_{ub}| = 0.0040$ and different values of C_{B_d} (see Eq. (54)) and $\bar{\Delta}_A^{\mu\mu}$ (see Eq. (53)). Black point: SM central value. The gray region represents the data.

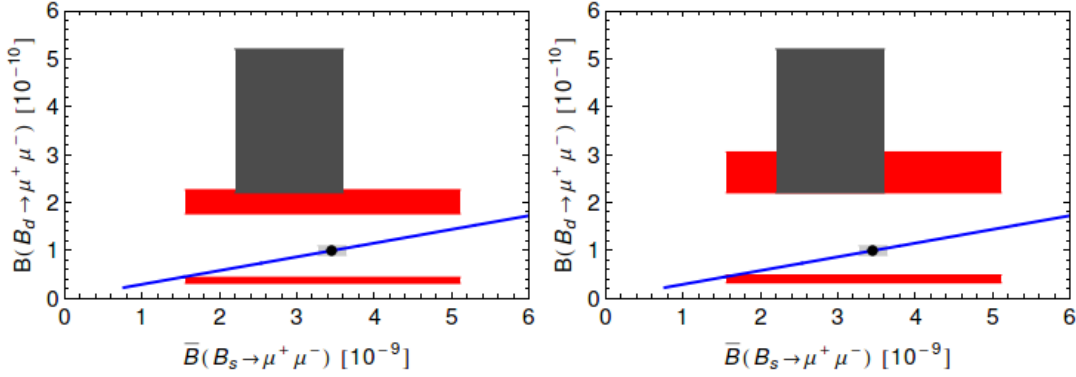


Figure 9: $\mathcal{B}(B_d \rightarrow \mu^+ \mu^-)$ versus $\bar{\mathcal{B}}(B_s \rightarrow \mu^+ \mu^-)$ for $|V_{ub}| = 0.0034$ (left) and $|V_{ub}| = 0.0040$ (right) and $C_{B_d} = 1.04 \pm 0.01$, $C_{B_s} = 1.00 \pm 0.01$, $\bar{\Delta}_A^{\mu\mu} = 1 \text{ TeV}^{-1}$, $0.639 \leq S_{\psi K_S} \leq 0.719$ and $-0.15 \leq S_{\psi\phi} \leq 0.15$. SM is represented by the light gray area with black dot and the CMFV prediction by the blue line. Dark gray region: Combined exp 1σ range $\bar{\mathcal{B}}(B_s \rightarrow \mu^+ \mu^-) = (2.9 \pm 0.7) \cdot 10^{-9}$ and $\mathcal{B}(B_d \rightarrow \mu^+ \mu^-) = (3.6_{-1.4}^{+1.6}) \cdot 10^{-10}$.

We find that in LHS1 case enhancement of $\mathcal{B}(B_d \rightarrow \mu^+\mu^-)$ corresponds for $S_{\psi K_S} \geq 0.66$ to low δ_{13} values but for $S_{\psi K_S} \leq 0.66$ both high and low ranges for δ_{13} can provide the enhancement. Note that in the case of enhancement $\mathcal{B}(B_d \rightarrow \mu^+\mu^-)$ overlaps with the data, while in the case of suppression it is roughly by a factor of two to three below its SM value. We should mention that we assume here that the two measurements of $B_s \rightarrow \mu^+\mu^-$ and $B_d \rightarrow \mu^+\mu^-$ are uncorrelated which is however not the case. This is shown for example in Fig. 2 of [29]. Consequently the areas in our Fig. 9 are exactly rectangular which would change if a correlation matrix for the combined LHCb and CMS data was included. This difference will only matter when the data improve.

Analogous structure would be found in $B_s \rightarrow \mu^+\mu^-$ case if we had chosen $C_{B_s} = 1.04$, but in this case as already noticed in [13] (see Fig. 21 of that paper) and also seen in the corresponding plot in Fig. 5 of the present paper, the impact of moving from $C_{B_s} < 1.0$ to $C_{B_s} > 1.0$ is much larger than in the B_d case and for $\bar{\Delta}_A^{\mu\bar{\mu}}(Z') \approx 1.0$ as required to fit the present data on $\mathcal{B}(B_d \rightarrow \mu^+\mu^-)$ one fails in this case to fit data for $\bar{\mathcal{B}}(B_s \rightarrow \mu^+\mu^-)$. In fact the black area most to the right in Fig. 5 for $C_{B_s} = 1.04$ would be red if we did not use the constraints (55). Also the blue region in this plot corresponding to $\bar{\Delta}_A^{\mu\bar{\mu}}(Z') = 0.5$ shows this structure.

For our choice of $C_{B_s} = 1.00$ the effects in question are mixed up in the two oases and there is no clear correspondence between a given oasis and enhancement or suppression of $\bar{\mathcal{B}}(B_s \rightarrow \mu^+\mu^-)$ when $S_{\psi\phi}$ is varied.

We concentrate now on the red regions in which $\mathcal{B}(B_d \rightarrow \mu^+\mu^-)$ is close to the data. Inspecting previous plots we find that the asymmetries $S_{\psi\phi}$ and $S_{\psi K_S}$ serve as coordinates in the horizontal and vertical direction, respectively and the departure from the SM point increases with the increasing $|S_{\psi K_S} - S_{\psi K_S}^{\text{NP}}|$ and similarly for the horizontal direction. Therefore

- In the LHS1 case the largest $\mathcal{B}(B_d \rightarrow \mu^+\mu^-)$ is obtained for the largest and lowest value of $S_{\psi K_S}$ in (57).
- In the LHS2 case it is found for the lowest value of $S_{\psi K_S}$.
- For LHS1 and LHS2 we find respectively

$$1.8 \cdot 10^{-10} \leq \mathcal{B}(B_d \rightarrow \mu^+\mu^-) \leq 2.3 \cdot 10^{-10}, \quad (\text{LHS1}). \quad (58)$$

$$2.2 \cdot 10^{-10} \leq \mathcal{B}(B_d \rightarrow \mu^+\mu^-) \leq 3.1 \cdot 10^{-10}, \quad (\text{LHS2}). \quad (59)$$

We also observe that in LHS2 even for $\bar{\Delta}_A^{\mu\bar{\mu}}(Z') = 0.5/\text{TeV}$ (see Fig. 8) this branching ratio can be by a factor of 1.5 – 1.9 larger than its SM value when $C_{B_d} = 1.04$.

Inspecting the plots in Figs. 5-8 we also observe that for $C_{B_d} = 1.00$ there would be no separation in two oases in the case of LHS1 and the values of $\mathcal{B}(B_d \rightarrow \mu^+\mu^-)$ would

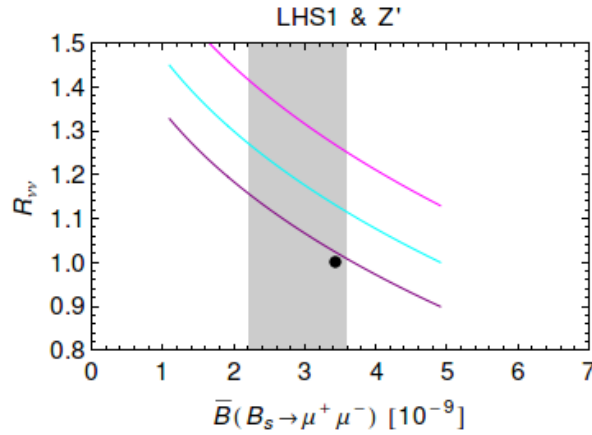


Figure 10: $R_{\nu\bar{\nu}}$ versus $\bar{\mathcal{B}}(B_s \rightarrow \mu^+ \mu^-)$ for $C_9^{\text{NP}} = -1.6$ (magenta), $C_9^{\text{NP}} = -0.8$ (cyan), $C_9^{\text{NP}} = -0.14$ (purple) and $-0.8 \leq C_{10}^{\text{NP}} \leq 1.8$.

be lower than in the example presented in Fig. 9 but the plot for LHS2 would hardly change. With decreasing C_{B_d} the LHS1 scenario is unable to reproduce the data for the branching ratio in question for $\bar{\Delta}_A^{\mu\mu}(Z') = 1.0/\text{TeV}$, while in the case of LHS2 the data for this branching ratio within 1σ can be reproduced provided $S_{\psi K_S}$ is low enough.

4.5 The $b \rightarrow s\nu\bar{\nu}$ Transitions

In the absence of right-handed currents one finds [61]

$$R_{\nu\bar{\nu}} \equiv \frac{\mathcal{B}(B \rightarrow K\nu\bar{\nu})}{\mathcal{B}(B \rightarrow K\nu\bar{\nu})_{\text{SM}}} = \frac{\mathcal{B}(B \rightarrow K^*\nu\bar{\nu})}{\mathcal{B}(B \rightarrow K^*\nu\bar{\nu})_{\text{SM}}} = \frac{\mathcal{B}(B \rightarrow X_s\nu\bar{\nu})}{\mathcal{B}(B \rightarrow X_s\nu\bar{\nu})_{\text{SM}}} = \frac{|X_L(B_s)|^2}{|\eta_X X_0(x_t)|^2}, \quad (60)$$

with $X_L(B_s)$ given in (44). The equality of these three ratios is an important test of the LHS scenario. The violation of them would imply the presence of right-handed couplings at work [61,67,68]. In the context of Z' models this is clearly seen in Fig. 20 of [14].

Using the $SU(2)_L$ relation in (45) we can now correlate these ratios with $\bar{\mathcal{B}}(B_s \rightarrow \mu^+ \mu^-)$ and C_9^{NP} . The power of this relation allows us to avoid the discussion of muon couplings at present even if knowing them would allow to correlate C_9^{NP} and C_{10}^{NP} .

In Fig. 10 we show $R_{\nu\bar{\nu}}$ versus $\bar{\mathcal{B}}(B_s \rightarrow \mu^+ \mu^-)$ for $C_9^{\text{NP}} = -1.6$ (magenta) and $C_9^{\text{NP}} = -0.8$ (cyan) and $-0.8 \leq C_{10}^{\text{NP}} \leq 1.8$. We observe an anti-correlation between these branching ratios as opposed to correlation found in [14]. But in the latter paper $\Delta_L^{\nu\bar{\nu}}(Z') = \Delta_A^{\mu\mu}(Z') = 0.5$ has been assumed. With the values of C_9^{NP} as used here these two couplings have opposite sign and anti-correlation follows. But the predicted NP effects in $R_{\nu\bar{\nu}}$ are rather small. The same conclusion has been reached in [26].

4.6 Comments on other NP models

The decays $B_{s,d} \rightarrow \mu^+ \mu^-$ have been studied in various models in the literature but in view of many parameters involved very often no clear cut conclusions can be made. Here we just want to mention four models where this can be done.

In the Littlest Higgs model with T-parity, $\overline{\mathcal{B}}(B_s \rightarrow \mu^+ \mu^-)$ can only be enhanced with respect to its SM value and this enhancement comes dominantly from the T-even sector [69]. Larger effects are possible in the case of $B_d \rightarrow \mu^+ \mu^-$ and the CMFV relation (34) as seen in Fig. 8 of [69] can be significantly violated, in particular for SM-like values of $S_{\psi\phi}$. Thus in LHT

$$R_{\mu\mu}(B_s) \equiv \frac{\mathcal{B}(B_s \rightarrow \mu^+ \mu^-)}{\mathcal{B}(B_s \rightarrow \mu^+ \mu^-)_{\text{SM}}} = 1.15 \pm 0.10, \quad 0.5 \leq r \leq 1.1 \quad (61)$$

showing that in this model $r < 1$ is favoured over $r > 1$ as indicated by the CMS and LHCb result in (35) although the values of r as given there cannot be reached. On the other hand the predicted enhancement of $\overline{\mathcal{B}}(B_s \rightarrow \mu^+ \mu^-)$ could turn out to be a problem for this model if data improve. We should remark that the operator structure in this model is as in LHS and it is a non-MFV model. But tree-level FCNCs are absent in this model.

Even if the presence of the fourth generation is unlikely or even excluded [70] it is interesting to observe that in the case of $S_{\psi\phi}$ as found by the LHCb $\overline{\mathcal{B}}(B_s \rightarrow \mu^+ \mu^-)$ is most likely suppressed and $\mathcal{B}(B_d \rightarrow \mu^+ \mu^-)$ enhanced so that the present data on these two branching ratios can be reproduced in this model. This is clearly seen in Figs. 4 and 5 of [71]. Thus if not for the difficulties of this model discussed in [70] the recent data on these decays could be a support for this model. For a recent discussion in this spirit see [72].

Next in the Randall-Sundrum model with custodial protection one finds [73]

$$R_{\mu\mu}(B_s) = 1.00 \pm 0.10, \quad 0.6 \leq r \leq 1.35 \quad (62)$$

with equal probability of r being suppressed or enhanced with respect to $r = 1$. Finally similar size of departures from CMFV have been identified recently within 331 models as can be seen in Fig. 12 of [74].

4.7 Comments on the size of reduced couplings

Our analysis did not make any assumptions on the diagonal couplings of Z' to quarks and in the case of charged leptons we did not assume the universality of lepton couplings so that Z' couplings to muons and electrons could be in principle different from each other. In fact as our recent analysis [74] shows, this violation of lepton universality is required for most interesting cases considered here by us as otherwise only the values

$\bar{\Delta}_A^{\mu\bar{\mu}}(Z') \leq 0.55$ would be allowed by LEP-II data [75]. For the vector couplings this bound is even stronger $\bar{\Delta}_V^{\mu\bar{\mu}}(Z') \leq 0.35$. We refer to section 7.2 of [74] for more details. These findings imply that the large enhancement of $\mathcal{B}(B_d \rightarrow \mu^+\mu^-)$ in LHS modes must be accompanied with breakdown of universality in Z' couplings to leptons.

5 The case of the SM Z

We will next consider the case of the SM Z boson with flavour violating couplings. An extensive analysis of this case has been performed in [14] and it is of interest to see how this scenario faces new data. In this case we have

$$M_Z = 91.2 \text{ GeV}, \quad \Delta_L^{\nu\bar{\nu}}(Z) = \Delta_A^{\mu\bar{\mu}}(Z) = 0.372, \quad \Delta_V^{\mu\bar{\mu}}(Z) = -0.028 \quad (63)$$

and consequently the reduced leptonic couplings are fixed:

$$\bar{\Delta}_L^{\nu\bar{\nu}}(Z) = \bar{\Delta}_A^{\mu\bar{\mu}}(Z) = 4.04/\text{TeV}, \quad \bar{\Delta}_V^{\mu\bar{\mu}}(Z) = -0.304/\text{TeV}. \quad (64)$$

We observe that $\bar{\Delta}_L^{\nu\bar{\nu}}(Z) = \bar{\Delta}_A^{\mu\bar{\mu}}(Z)$ is much larger than considered presently by us in the case of Z' , while as we will soon see $\bar{\Delta}_V^{\mu\bar{\mu}}(Z)$ turns out to be too small to give the values C_9^{NP} in (30). In fact as seen in the right panel of Fig. 11 its most negative value is around -0.14 . It is this value that we have used in Fig. 10 to show that in the Z -case the effects in $b \rightarrow s\nu\bar{\nu}$ transitions are even smaller than in the Z' -case.

What remains to be done is to fix the FCNC couplings of Z to quarks by imposing the constraints from ΔM_s and $S_{\psi\phi}$. This has been already done in Section 9 in [14] with the result that $\bar{\mathcal{B}}(B_s \rightarrow \mu^+\mu^-)$ is always larger than its SM value and mostly above the data known at that time that decreased significantly since then. Moreover it has been shown that the constraints (55) could not be satisfied. However, in [14] $C_{B_s} = 0.927$ has been used as this was hinted by lattice data at that time. Requiring the agreement with the data on ΔM_s within $\pm 5\%$ implied the Zbs coupling to be too large in the presence of a large coupling $\bar{\Delta}_A^{\mu\bar{\mu}}(Z)$ in (64) so that these constraints could not be satisfied. But with the new lattice input even $C_{B_s} = 1.00 \pm 0.01$ is fine and the coupling $\bar{\Delta}_L^{sb}(Z)$ is allowed to be much smaller so that data on $\Delta F = 2$ observables and $\bar{\mathcal{B}}(B_s \rightarrow \mu^+\mu^-)$ can be satisfied while being consistent with the constraints in (55). However it turns out that only the case of $C_{B_s} = 1.00 \pm 0.01$ is admitted and this implies that not only ΔM_s but also $S_{\psi\phi}$ has to be close to their SM values (see Fig. 11). Still as we will see significant deviations of $\bar{\mathcal{B}}(B_s \rightarrow \mu^+\mu^-)$ from the SM prediction are possible because of very large value of $\bar{\Delta}_A^{\mu\bar{\mu}}(Z)$. Improved lattice calculations will tell us whether this scenario works.

Let us then study the case of the $B_d \rightarrow \mu^+\mu^-$ decay. As now the coupling $\bar{\Delta}_A^{\mu\bar{\mu}}(Z)$ is fixed it is easier to see what happens for different values of C_{B_d} . In [14] also $C_{B_d} = 0.927$ has been considered implying large enhancements of $\mathcal{B}(B_d \rightarrow \mu^+\mu^-)$, which as seen in Fig. 28 of that paper are in the LHS1 scenario on top of the CMS and LHCb data but a

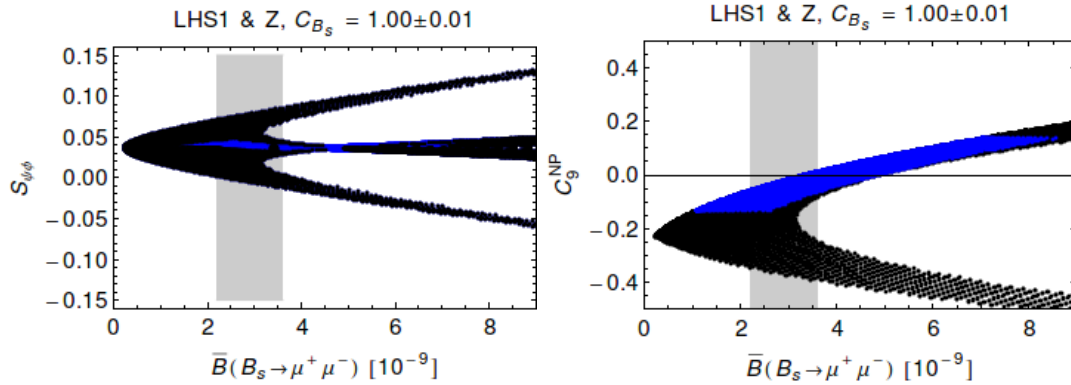


Figure 11: $S_{\psi\phi}$ versus $\bar{\mathcal{B}}(B_s \rightarrow \mu^+\mu^-)$ (left) and C_9^{NP} versus $\bar{\mathcal{B}}(B_s \rightarrow \mu^+\mu^-)$ (right) for $C_{B_s} = 1.00 \pm 0.01$. The black points violates the bounds for C_{10}^{NP} (see Eq. (55)).

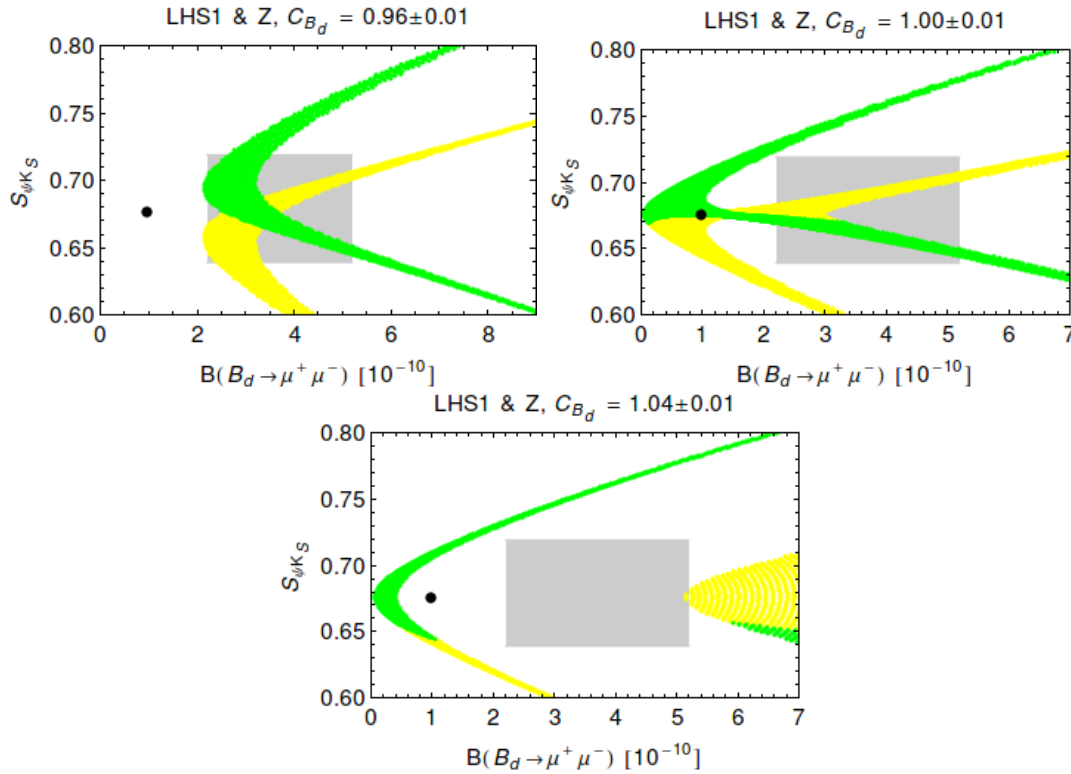


Figure 12: $S_{\psi K_S}$ versus $\mathcal{B}(B_d \rightarrow \mu^+\mu^-)$ for $C_{B_s} = 0.96 \pm 0.01$, $C_{B_s} = 1.00 \pm 0.01$ and $C_{B_s} = 1.04 \pm 0.01$ in LHS1. The yellow and green points correspond to the different oases that differ by π in δ_{13} .

bit higher, although still consistent with the latter, for the LHS2. We could even claim that our prediction has been confirmed by CMS and LHCb data but in view of large experimental errors and modified lattice results we will update our analysis.

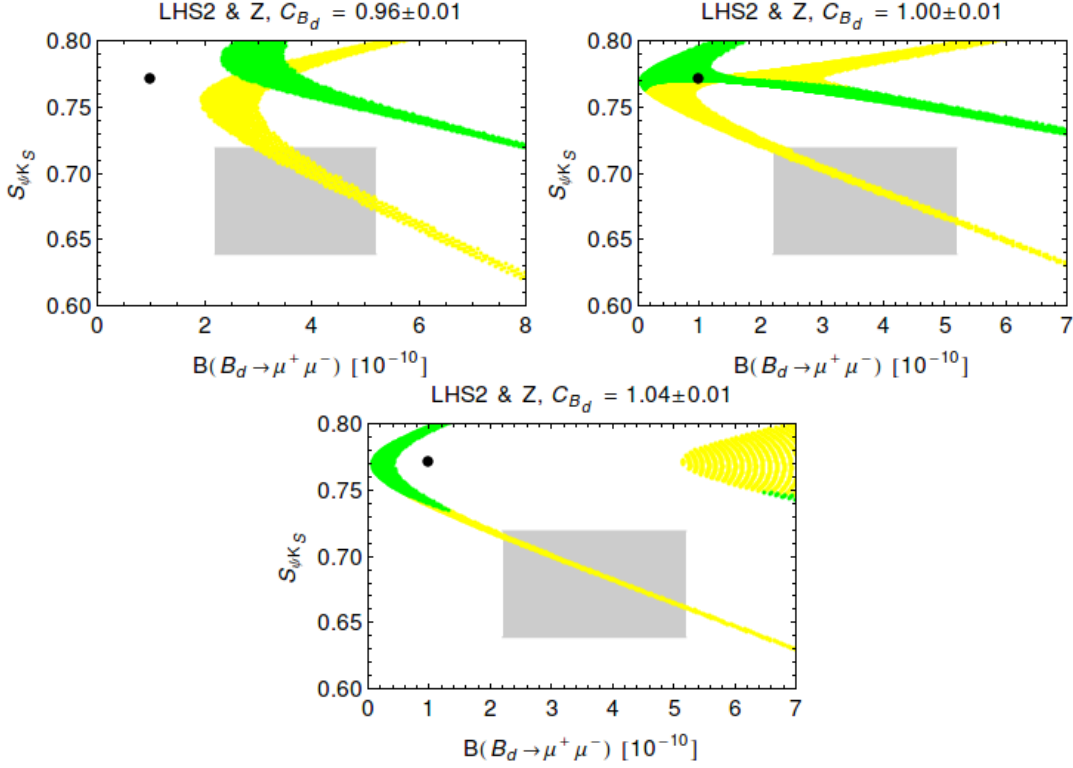


Figure 13: $S_{\psi K_S}$ versus $\mathcal{B}(B_d \rightarrow \mu^+ \mu^-)$ for $C_{B_d} = 0.96 \pm 0.01$, $C_{B_d} = 1.00 \pm 0.01$ and $C_{B_d} = 1.04 \pm 0.01$ in LHS2. The yellow and green points correspond to the different oases that differ by π in δ_{13} .

As we fixed $C_{B_s} = 1.00 \pm 0.01$, C_{B_d} should not differ by too much from this value in order to agree with the data on the ratio $\Delta M_s / \Delta M_d$. Therefore we consider only the cases

$$C_{B_d} = 0.96 \pm 0.01, \quad C_{B_d} = 1.00 \pm 0.01, \quad C_{B_d} = 1.04 \pm 0.01. \quad (65)$$

and show for them in Figs. 12 and 13 the correlation between $S_{\psi K_S}$ and $\mathcal{B}(B_d \rightarrow \mu^+ \mu^-)$ in LHS1 and LHS2 scenarios for $|V_{ub}|$. Here we also distinguish between the two different oases (yellow and green points). The following observations can be made on the basis of these results:

- In LHS1 for $C_{B_d} = 0.96 \pm 0.01$ and $C_{B_d} = 1.00 \pm 0.01$ a very good agreement with experiment for both oases can be obtained, but only for $C_{B_d} = 0.96 \pm 0.01$ is $\mathcal{B}(B_d \rightarrow \mu^+ \mu^-)$ forced to be enhanced. For $C_{B_d} = 1.04 \pm 0.01$ it is outside the gray area.
- In LHS2 where NP must be present to reduce the value of $S_{\psi K_S}$, there is an agreement for all three values of C_{B_d} but only in the yellow oasis (low δ_{13}). Note that in the Z -case the muon coupling is fixed and it is the yellow oasis which is chosen by the data.

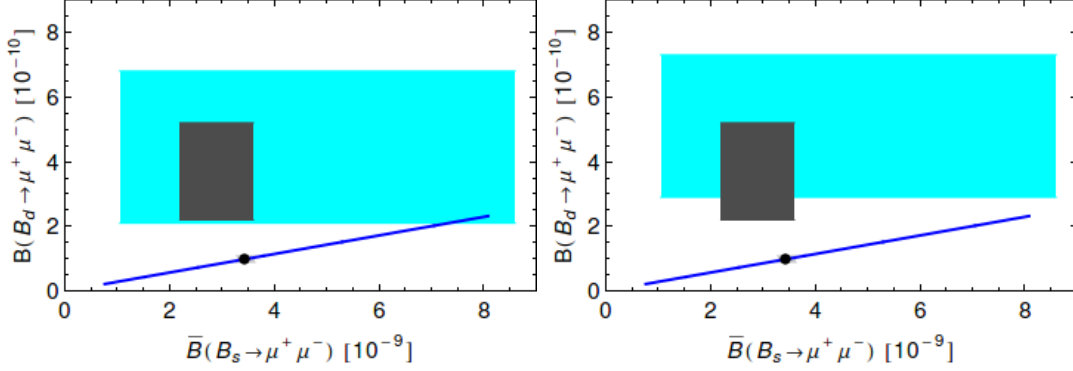


Figure 14: $\mathcal{B}(B_d \rightarrow \mu^+ \mu^-)$ versus $\bar{\mathcal{B}}(B_s \rightarrow \mu^+ \mu^-)$ for $|V_{ub}| = 0.0034$ (left) and $|V_{ub}| = 0.0040$ (right) and $C_{B_d} = 0.96 \pm 0.01$, $C_{B_s} = 1.00 \pm 0.01$, $0.639 \leq S_{\psi K_s} \leq 0.719$ and $-0.15 \leq S_{\psi\phi} \leq 0.15$. SM is represented by the light gray area with black dot. Dark gray region: Combined exp 1σ range $\bar{\mathcal{B}}(B_s \rightarrow \mu^+ \mu^-) = (2.9 \pm 0.7) \cdot 10^{-9}$ and $\mathcal{B}(B_d \rightarrow \mu^+ \mu^-) = (3.6_{-1.4}^{+1.6}) \cdot 10^{-10}$.

We conclude therefore that the Z boson with left-handed flavour violating couplings can reproduce the CMS and LHCb data for $B_{s,d} \rightarrow \mu^+ \mu^-$ while being consistent with present constraints from ΔM_d and $S_{\psi K_s}$. Interestingly in the LHS1 scenario there is a preference for $C_{B_d} \leq 1.0$ while all values work in the case of LHS2. If the branching ratio decreases in the future below $2 \cdot 10^{-10}$, LHS1 will be favoured but in that case the lower limit on C_{B_d} will be higher than 0.96.

The result analogous to the plots in Fig. 9 is shown in Fig. 14. As an example we have chosen $C_{B_d} = 0.96 \pm 0.01$ and $C_{B_s} = 1.00 \pm 0.01$ for both LHS1 and LHS2. For LHS1 and LHS2 we find respectively

$$2.1 \cdot 10^{-10} \leq \mathcal{B}(B_d \rightarrow \mu^+ \mu^-) \leq 6.8 \cdot 10^{-10}, \quad (\text{LHS1}). \quad (66)$$

$$2.9 \cdot 10^{-10} \leq \mathcal{B}(B_d \rightarrow \mu^+ \mu^-) \leq 7.3 \cdot 10^{-10}, \quad (\text{LHS2}). \quad (67)$$

and in both cases

$$1.2 \cdot 10^{-10} \leq \bar{\mathcal{B}}(B_s \rightarrow \mu^+ \mu^-) \leq 7.2 \cdot 10^{-10}. \quad (68)$$

Compared with the plots in Fig. 9, these plots could imply that it is more natural to reproduce the present data for $B_d \rightarrow \mu^+ \mu^-$ in the case of Z rather than Z' scenario. However we should remember that as seen in Figs. 7 and 8 higher values of $B_d \rightarrow \mu^+ \mu^-$ branching ratios can be obtained in the latter scenario by increasing the coupling $\bar{\Delta}_A^{\mu\bar{\mu}}(Z')$ above the unity.

So far so good. In view of the condition $C_{B_s} = 1.00 \pm 0.01$ required by the constraints (55) combined with the $B_s \rightarrow \mu^+ \mu^-$ data the couplings $\bar{\Delta}_L^{sb}(Z)$ are too small to compensate the smallness of $\bar{\Delta}_V^{\mu\bar{\mu}}(Z)$ in the evaluation of C_9^{NP} (see Fig. 11). Consequently, the values in (30) cannot be reproduced. Thus the only hope for the Z -scenario is a very significant reduction of C_9^{NP} in the future.

6 Comments on a real C_9^{NP} and right-handed couplings

6.1 Real C_9^{NP}

The recent $B \rightarrow K^* \mu^+ \mu^-$ anomalies imply according to [26, 34] the range for $C_9^{\text{NP}}(B_s)$ given in (30) and moreover this contribution could come from a Z' exchange. Here we would like to collect the implications of this possibility for the LHS. These are

- Unique enhancement of ΔM_s with respect to its SM value implying that this scenario can only be valid for $C_{B_s} > 1.0$. As we have seen in the previous section this is not favoured by the present data on $B_{s,d} \rightarrow \mu^+ \mu^-$ but cannot be excluded due to large errors on experimental $B_{s,d} \rightarrow \mu^+ \mu^-$ branching ratios. Future lattice calculations will tell us whether $C_{B_s} > 1.0$ is true. In fact the most recent values in (52) favour slightly such values.
- As in this case $\delta_{23} = \beta_s$ or $\delta_{23} = \beta_s + \pi$, the asymmetry $S_{\psi\phi}$ equals the SM one. We are in the scenario for SM-like $S_{\psi\phi}$ with the restriction $C_{B_s} > 1.0$ and these are the *magenta* points in Figs. 1 and 4. Consequently the CP-asymmetries A_7 and A_8 in $B \rightarrow K^* \mu^+ \mu^-$ vanish.
- Due to the relation (24) there is a strict correlation between $\overline{\mathcal{B}}(B_s \rightarrow \mu^+ \mu^-)$ and $C_9^{\text{NP}}(B_s)$ that depends on the values of the ratio $\overline{\Delta}_A^{\mu\bar{\mu}}(Z')/\overline{\Delta}_V^{\mu\bar{\mu}}(Z')$. We show this correlation in the left panel of Fig. 15. In the right panel we show using (36) C_{B_s} as a function of a real $C_9^{\text{NP}}(B_s)$ for different values of $\overline{\Delta}_V^{\mu\bar{\mu}}(Z')$ so that some correlation between ΔM_s and $\overline{\mathcal{B}}(B_s \rightarrow \mu^+ \mu^-)$ is present. The main message from this plot is that combined data for $\overline{\mathcal{B}}(B_s \rightarrow \mu^+ \mu^-)$ and C_9^{NP} favour

$$0 \leq \frac{\overline{\Delta}_A^{\mu\bar{\mu}}(Z')}{\overline{\Delta}_V^{\mu\bar{\mu}}(Z')} \leq 1.0, \quad (69)$$

implying that these two couplings should have the same sign.

- While in the B_s system there are some similarities of this scenario with the CMFV models, LHS differs in the presence of a real $C_9^{\text{NP}}(B_s)$ from CMFV as NP physics with new complex phases can enter B_d and K systems. Moreover as we have seen the present data on $\mathcal{B}(B_d \rightarrow \mu^+ \mu^-)$ favour $\overline{\Delta}_A^{\mu\bar{\mu}}(Z') \approx 1.0$ and this can also be correlated with the results in Fig. 15.

6.2 Right-handed currents

In [14] we have analyzed in addition to LHS scenario also RHS scenario in which only right-handed Z' couplings were present and two scenarios (LRS and ALRS) with both

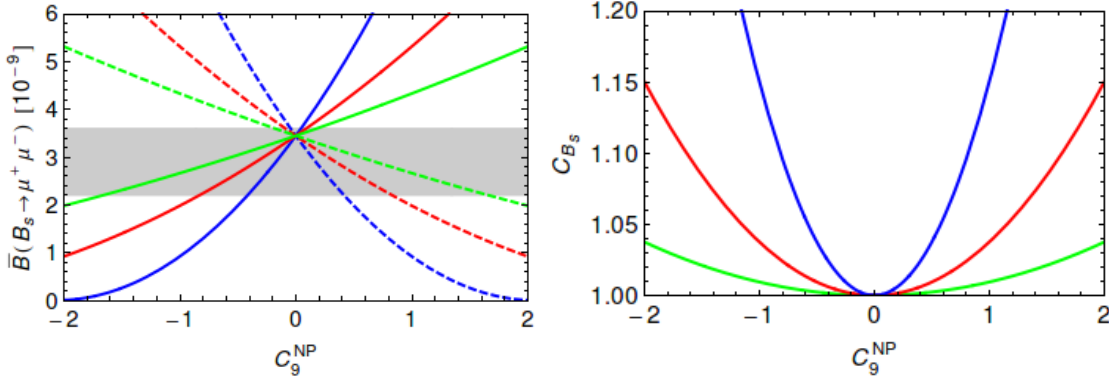


Figure 15: $\bar{\mathcal{B}}(B_s \rightarrow \mu^+ \mu^-)$ and C_{B_s} versus a real C_9^{NP} . Left: $\bar{\Delta}_A^{\mu\bar{\mu}}/\bar{\Delta}_V^{\mu\bar{\mu}} = -2$ (blue dashed), -1 (red dashed), -0.5 (green dashed), 0.5 (green), 1 (red) and 2 (blue). Right: $\bar{\Delta}_V^{\mu\bar{\mu}} = \pm 0.5 \text{ TeV}^{-1}$ (blue), $\pm 1 \text{ TeV}^{-1}$ (red) and $\pm 2 \text{ TeV}^{-1}$ (green).

left-handed and right-handed couplings satisfying the relations

$$\Delta_L^{qb}(Z') = \Delta_R^{qb}(Z'), \quad \Delta_L^{qb}(Z') = -\Delta_R^{qb}(Z'), \quad (70)$$

respectively. Our analysis included complex couplings but in the spirit of this section and to relate to the analyses in [26,34] let us assume here that these couplings have the same phases modulo π so that resulting Wilson coefficients remain real.

To an excellent approximation the shift ΔS in (14) is now obtained by making the following replacement

$$(\Delta_L^{bs}(Z'))^2 \rightarrow (\Delta_L^{bs}(Z'))^2 + (\Delta_R^{bs}(Z'))^2 + \kappa \Delta_L^{bs}(Z') \Delta_R^{bs}(Z'), \quad (71)$$

where

$$\kappa = 2 \frac{\langle Q_1^{\text{LR}}(\mu_{Z'}) \rangle}{\langle Q_1^{\text{VLL}}(\mu_{Z'}) \rangle} \approx -10.3 \quad (72)$$

exhibits the known fact that the matrix elements of LR operators are strongly enhanced with respect to VLL operators that are solely responsible for $\Delta F = 2$ effects in the SM and LHS scenario. We would like to add that due to different anomalous dimensions of LR and VLL operators, κ increases with increasing $\mu_{Z'} = \mathcal{O}(M_{Z'})$. The value given in (72) corresponds to $\mu_{Z'} = 1 \text{ TeV}$. For more details, in particular NLO corrections, we refer to [1,40]. Analogous expressions for other meson systems exist. Now as seen in Table 2 of [1] model independently κ is *negative* which has an impact on the signs and size of NP contributions to ΔM_s .

We make the following observations following more detailed discussion in [1,14]:

- In the case of the RHS scenario the $\Delta F = 2$ constraints are exactly the same as in the LHS scenario but this time on the right-handed couplings.

- In the case of the LRS scenario with the NP phase aligned to the SM one, NP contribution to ΔM_s is strictly *negative* as opposed to the LHS scenario and because of the κ -enhancement the coupling $\bar{\Delta}_L^{sb}(Z')$ must be suppressed by a factor $\sqrt{8}$ relatively to the LHS or RHS case. For fixed leptonic couplings NP effects in $b \rightarrow s\mu^+\mu^-$ transitions are expected to be smaller than in LHS scenario. As the contribution is negative anyway, in the case of establishing $C_{B_s} > 1.00$ this scenario will be ruled out.
- In the case of ALRS scenario with the NP phase aligned to the SM one, NP contribution to ΔM_s is strictly *positive* as in the LHS scenario but because of the κ -enhancement the coupling $\bar{\Delta}_L^{sb}(Z')$ must be suppressed by a factor $\sqrt{12}$ relatively to the LHS or RHS case. For fixed leptonic couplings NP effects in $b \rightarrow s\mu^+\mu^-$ transitions are expected to be smaller than in LHS scenario. As the contribution is positive in the case of establishing $C_{B_s} < 1.00$ this scenario will be ruled out.

Concerning $B_{s,d} \rightarrow \mu^+\mu^-$, as emphasized in [14], NP effects vanish in the LRS scenario independently of the leptonic couplings. But it could be that the quark couplings in $B_s \rightarrow \mu^+\mu^-$ belong to the LRS scenario and this is the reason why the data are close to the SM prediction, while this is not the case for the quark couplings in $B_d \rightarrow \mu^+\mu^-$. In the case of ALRS scenario NP does contribute to $B_{s,d} \rightarrow \mu^+\mu^-$ and the fact that LH and RH couplings enter the decay amplitude with the same sign compensates partly the suppression of quark couplings due to enhanced $\Delta F = 2$ matrix elements.

Let us next investigate $B_d \rightarrow K^*\mu^+\mu^-$ in these scenarios. We concentrate here on three angular observables F_L , S_4 and S_5 introduced in [76] that are particularly sensitive to NP contributions. Useful approximate formulae for them in terms of Wilson coefficients have been recently presented in [26]. These formulae neglect interferences between NP contributions which is justified in view of small room left for these contributions in the data. Applied to Z' models these formulae are as follows:

$$\langle F_L \rangle_{[1,6]} \approx 0.77 + 0.05C_9^{\text{NP}} - 0.04C'_9 + 0.04C'_{10} \quad (73)$$

$$\langle S_4 \rangle_{[14.2,16]} \approx 0.29 - 0.02C'_9 + 0.03C'_{10}. \quad (74)$$

$$\langle S_5 \rangle_{[1,6]} \approx -0.14 - 0.09C_9^{\text{NP}} - 0.03C'_9 + 0.10C'_{10}. \quad (75)$$

Here the subscripts on the l.h.s of these formulae indicate for which bin in q^2 these equations and corresponding data given below apply. In order not to obuse notations we will drop these subscripts in what follows.

Also in RHS, LRS and ALRS scenarios, NP contributions to the dipole operator can be neglected [14] and this reduction of the number of relevant Wilson coefficients together with the absence of new CP-violating phases allows to derive correlations between these three observables in question as we will see soon. Here the primed coefficients are obtained from the unprimed ones by replacing $\Delta_L^{qb}(Z')$ by $\Delta_R^{qb}(Z')$.

It should be emphasized that the numerical values in (73)-(75) are subject to hadronic uncertainties. Therefore, even if in our numerical analysis of various correlations we will use these values, we collect in the Appendix A general formulae for these correlations. This should allow to update these correlations if the numerical values in (73)-(75) will be modified. Moreover, from the Appendix A one can derive correlations for the basis of observables proposed in [77] by using the dictionary [26]

$$S_3 = \frac{1}{2}F_T P_1, \quad S_4 = \frac{1}{2}F_{LT} P'_4, \quad S_5 = \frac{1}{2}F_{LT} P'_5, \quad (76)$$

where $F_{LT} = \sqrt{F_L(1 - F_L)}$.

The first terms in (73)-(75) are SM predictions. The estimate of uncertainties vary from paper to paper. We quote here the results from [26]

$$\langle F_L \rangle = 0.77 \pm 0.04, \quad \langle S_4 \rangle = 0.29 \pm 0.07, \quad \langle S_5 \rangle = -0.14 \pm 0.02. \quad (77)$$

For other estimates see [38,77]. In particular in [38] much larger error has been assigned to $\langle S_5 \rangle$.

Concerning the data, the ones quoted in [26] and given by

$$\langle F_L \rangle = 0.59 \pm 0.08, \quad \langle S_4 \rangle = -0.07 \pm 0.11, \quad \langle S_5 \rangle = 0.10 \pm 0.10, \quad (78)$$

are based on the LHCb data for P'_4 and P'_5 [32] and the average of the data from Belle, Babar, CDF, CMS, ATLAS and LHCb on F_L which as discussed in the appendix of [26] are not in full agreement with each other. We find that the weighted average of the most accurate data from LHCb [31] and CMS [33] is $\langle F_L \rangle = 0.66 \pm 0.07$, without basically no change in S_4 and S_5 . In our plots we will show both ranges on $\langle F_L \rangle$. Note that the definition of S_4 differs from the LHCb definition by sign.

The central values, in particular for S_4 and S_5 differ from SM predictions, in particular the sign of $\langle S_5 \rangle$ is opposite. But the uncertainties both in theory and experiment are sizable. Still this pattern of deviations could be a sign of NP at work.

Having this formulae at hand it is evident that in LHS, RHS, LRS and ALRS in which some of the coefficients in question are related to each other correlations between these three angular observables are present. In the rest of this section we will exhibit these correlations analytically and graphically neglecting all theoretical uncertainties which certainly are not small. Our goal is modest: we just want to uncover these correlations as this has not been done in the literature, leaving a sophisticated numerical analysis for the future when the data stabilize and a consensus between theorists on the hadronic uncertainties will be reached. We should also warn the reader that when our results in Z' models differ from SM values by much, the neglect of interferences between different NP contributions cannot be fully justified but at the semi-quantitative level the presented plots should represent what is going on.

We can now specify the formulae in (73)-(74) to the four scenarios in question:

LHS:

$$\langle F_L \rangle \approx 0.77 + 0.05C_9^{\text{NP}}, \quad (79)$$

$$\langle S_4 \rangle \approx 0.29, \quad (80)$$

$$\langle S_5 \rangle \approx -0.14 - 0.09C_9^{\text{NP}}. \quad (81)$$

Eliminating C_9^{NP} from these expressions in favour of $\langle S_5 \rangle$ we find

$$\langle F_L \rangle = 0.69 - 0.56\langle S_5 \rangle, \quad (82)$$

which shows analytically the point made in [26, 34] that NP effects in F_L and S_5 are anti-correlated as observed in the data.

We show this correlation in the upper left panel in Fig. 16 together with the data. We observe that for negative $C_9^{\text{NP}} = \mathcal{O}(1)$ one can obtain agreement with the data for these two observables provided such values are also allowed by other constraints. We also observe that for the larger value of $\langle F_L \rangle$ (dark grey) it is easier for LHS to describe the data. On the other hand the value of $\langle S_4 \rangle$ remains SM-like and is significantly larger than indicated by the data in (78). The departure of $\langle S_4 \rangle$ from the SM value would be a sign of right-handed currents at work. In [26] it has been concluded that it is difficult to find any NP model which could explain the present data on $\langle S_4 \rangle$ and similar conclusion has been reached in [78]. However, we will keep this observable in our presentation in order to be prepared for future data.

RHS:

$$\langle F_L \rangle \approx 0.77 - 0.04C'_9 + 0.04C'_{10}, \quad (83)$$

$$\langle S_4 \rangle \approx 0.29 - 0.02C'_9 + 0.03C'_{10}. \quad (84)$$

$$\langle S_5 \rangle \approx -0.14 - 0.03C'_9 + 0.10C'_{10}. \quad (85)$$

Eliminating C'_{10} from these expressions we find

$$\langle F_L \rangle = 0.826 + 0.40\langle S_5 \rangle - 0.028C'_9, \quad (86)$$

$$\langle F_L \rangle = 0.38 + 1.33\langle S_4 \rangle - 0.013C'_9. \quad (87)$$

As seen in Fig. 17 NP effects in F_L and S_5 are correlated with each other and this scenario cannot describe the data even if C'_9 is positive and as large as 2, which is

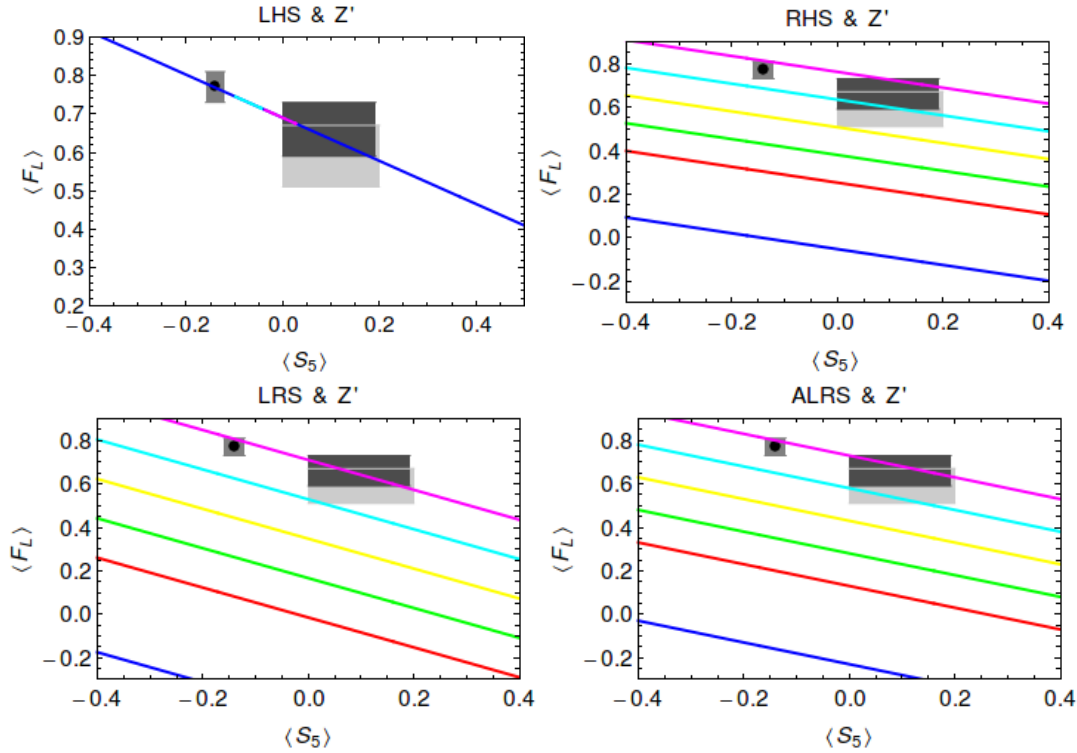


Figure 16: $\langle F_L \rangle$ versus $\langle S_5 \rangle$ in LHS, RHS, LRS and ALRS. For LHS we have $\langle S_4 \rangle = 0$ and the magenta line corresponds to $C_9^{\text{NP}} = -1.6 \pm 0.3$ and the cyan line to $C_9^{\text{NP}} = -0.8 \pm 0.3$ as in (30). In the other scenarios (RHS, LRS, ALRS) we choose $\langle S_4 \rangle = -0.02$ (blue, corresponds to the experimental central value), 0.1 (red), 0.15 (green), 0.2 (yellow), 0.25 (cyan) and 0.3 (magenta). The light gray area corresponds to the experimental range in (78) and in the dark gray area we changed $\langle F_L \rangle$ to 0.66 ± 0.07 which also slightly change $\langle S_{4,5} \rangle$ by a factor 0.963. The light gray line indicates where the light gray area stops. The black point and the gray box correspond to the SM predictions from (77).

not allowed by other constraints [26]. Thus in agreement with [26, 34], right-handed currents alone are not able to explain the anomalies in question.

Finally eliminating C_9' we find a triple correlation

$$\langle F_L \rangle = -0.019 - 0.36\langle S_5 \rangle + 2.55\langle S_4 \rangle. \quad (88)$$

We show this correlation in the right upper panel of Fig. 16. The message in this plot is clear. One cannot reproduce the present data in (78).

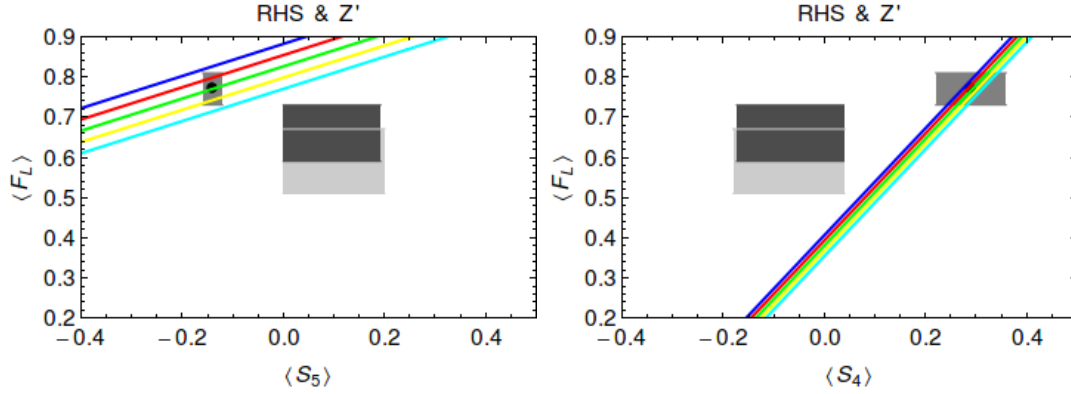


Figure 17: $\langle F_L \rangle$ versus $\langle S_5 \rangle$ and $\langle S_4 \rangle$ in RHS for different values of C_9' : -2 (blue), -1 (red), 0 (green), 1 (yellow) and 2 (cyan). The light gray area corresponds to the experimental range in (78) and in the dark gray area we changed $\langle F_L \rangle$ to 0.66 ± 0.07 which also slightly change $\langle S_{4,5} \rangle$ by a factor 0.963 . The light gray line indicates where the light gray area stops. The black point and the gray box correspond to the SM predictions from (77).

LRS:

As in this scenario the primed and unprimed coefficients are equal to each other we find

$$\langle F_L \rangle \approx 0.77 + 0.01C_9^{\text{NP}} + 0.04C_{10}^{\text{NP}}, \quad (89)$$

$$\langle S_4 \rangle \approx 0.29 - 0.02C_9^{\text{NP}} + 0.03C_{10}^{\text{NP}}. \quad (90)$$

$$\langle S_5 \rangle \approx -0.14 - 0.12C_9^{\text{NP}} + 0.10C_{10}^{\text{NP}}, \quad (91)$$

where we used $C_{10}^{\text{NP}} = C_{10}'$. Note, that in spite of the appearance of C_{10}^{NP} there is no constraint from $B_s \rightarrow \mu^+ \mu^-$ as NP contribution to this decay vanishes in this scenario, except that if future data will disagree with the SM prediction for this decay, LRS will not be able to explain this.

Eliminating C_{10}^{NP} from these expressions we find

$$\langle F_L \rangle = 0.826 + 0.40\langle S_5 \rangle + 0.058C_9^{\text{NP}}, \quad (92)$$

$$\langle F_L \rangle = 0.38 + 1.33\langle S_4 \rangle + 0.037C_9^{\text{NP}}. \quad (93)$$

We show these correlations in Fig. 18, where different colours represent different values of C_9^{NP} . Evidently, it is impossible to describe the data in these two plots simultaneously with the same value of this coefficient. While in the left-plot a sufficiently large negative value of C_9^{NP} would help in explaining the data, in the right plot a positive value is required. This is also seen in Fig. 16 where we show the triple correlation which one

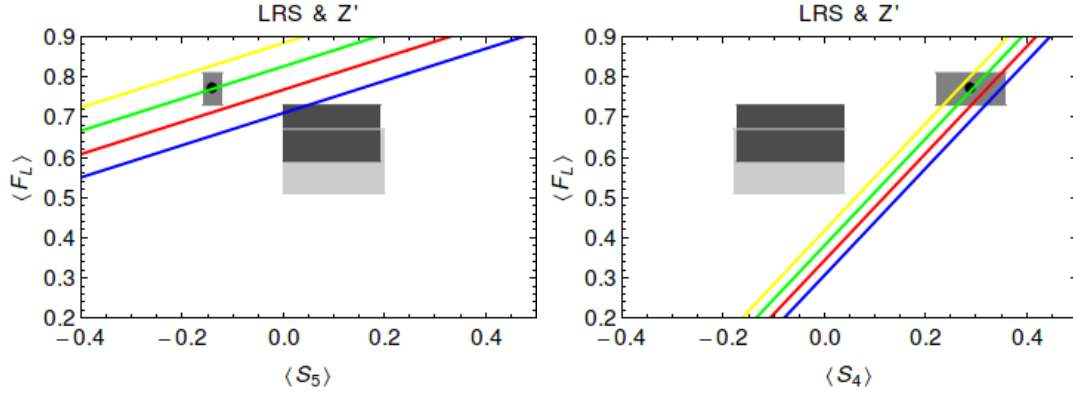


Figure 18: $\langle F_L \rangle$ versus $\langle S_5 \rangle$ and $\langle S_4 \rangle$ in LRS for different values of C_9^{NP} : -2 (blue), -1 (red), 0 (green) and 1 (yellow). The light gray area corresponds to the experimental range in (78) and in the dark gray area we changed $\langle F_L \rangle$ to 0.66 ± 0.07 which also slightly change $\langle S_{4,5} \rangle$ by a factor 0.963 . The light gray line indicates where the light gray area stops. The black point and the gray box correspond to the SM predictions from (77).

obtains after eliminating C_9^{NP}

$$\langle F_L \rangle = -0.38 - 0.688\langle S_5 \rangle + 3.63\langle S_4 \rangle. \quad (94)$$

ALRS:

As in this scenario the primed and unprimed coefficients differ by sign we find

$$\langle F_L \rangle \approx 0.77 + 0.09C_9^{\text{NP}} - 0.04C_{10}^{\text{NP}}, \quad (95)$$

$$\langle S_4 \rangle \approx 0.29 + 0.02C_9^{\text{NP}} - 0.03C_{10}^{\text{NP}}, \quad (96)$$

$$\langle S_5 \rangle \approx -0.14 - 0.06C_9^{\text{NP}} - 0.10C_{10}^{\text{NP}}, \quad (97)$$

where we used $C_{10}^{\text{NP}} = -C'_{10}$. We find in this case the following correlations

$$\langle F_L \rangle = 0.826 + 0.40\langle S_5 \rangle + 0.114C_9^{\text{NP}}, \quad (98)$$

$$\langle F_L \rangle = 0.38 + 1.33\langle S_4 \rangle + 0.063C_9^{\text{NP}}. \quad (99)$$

In fact this scenario is rather close to the one investigated numerically in [26]. We show these correlations in Fig. 19. The one between $\langle F_L \rangle$ and $\langle S_4 \rangle$ is basically unchanged relatively to the LRS case while the one between $\langle F_L \rangle$ and $\langle S_5 \rangle$ appears to be in a better shape when compared with the data. In fact as emphasized in [26] it is easier

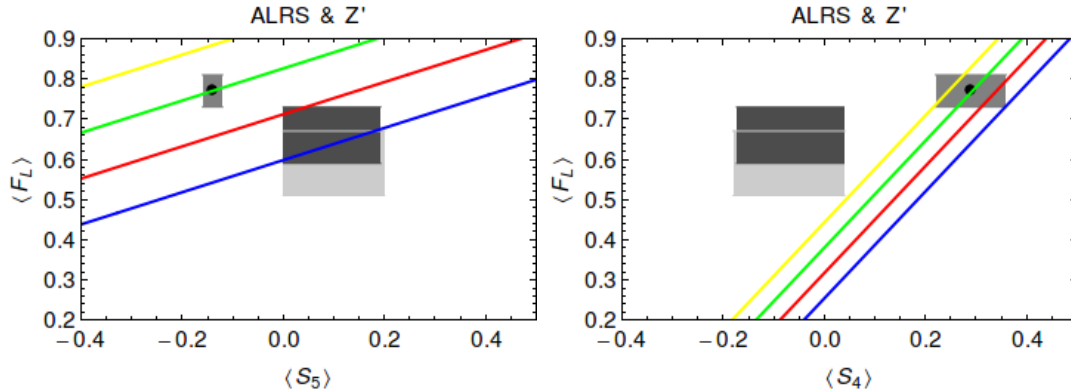


Figure 19: $\langle F_L \rangle$ versus $\langle S_5 \rangle$ and $\langle S_4 \rangle$ in ALRS for different values of C_9^{NP} : -2 (blue), -1 (red), 0 (green) and 1 (yellow). The light gray area corresponds to the experimental range in (78) and in the dark gray area we changed $\langle F_L \rangle$ to 0.66 ± 0.07 . The light gray line indicates where the light gray area stops. The black point and the gray box correspond to the SM predictions from (77).

to obtain the agreement with the data on $\langle F_L \rangle$ and $\langle S_5 \rangle$ by including a non-vanishing C_9' in addition to C_9^{NP} . As seen in the left plot of Fig. 4 in the latter paper, the data on A_{FB} and $B \rightarrow K\mu^+\mu^-$ favour C_9' to be of similar magnitude as C_9^{NP} but having opposite sign and this is our ALRS scenario.

Finally, we find the triple correlation

$$\langle F_L \rangle = -0.17 - 0.50\langle S_5 \rangle + 3.00\langle S_4 \rangle, \quad (100)$$

which we show in the lower right panel in Fig. 16. Again we observe the problem with describing the data on $\langle S_4 \rangle$.

Clearly a complete analysis must include constraints on the values of C_9^{NP} from other observables but such an analysis in the scenarios with right-handed currents is beyond the scope of the present paper. We refer to [26] for a sophisticated model independent numerical analysis of such scenarios which also involve the coefficients of the dipole operators which in Z' models are very suppressed.

The summary of this short excursion in the world of right-handed currents is as follows:

- The finalists in the competition between these four scenarios are LHS and ALRS and in agreement with [26] the present data on $\langle F_L \rangle$ and $\langle S_5 \rangle$ seem to favour ALRS over LHS.
- In order for these finalists to work the future experimental value of $\langle S_4 \rangle$ must be SM-like. This is in particular the case of LHS scenario. In ALRS this implies as seen in (74)

$$C_{10}^{\text{NP}} \approx \frac{2}{3}C_9^{\text{NP}} \quad (101)$$

and the correlation with $B_s \rightarrow \mu^+ \mu^-$ decay. We find then that $\bar{\mathcal{B}}(B_s \rightarrow \mu^+ \mu^-) \geq 4.6 \cdot 10^{-9}$.

In order to understand this result let us recall that with real NP contributions to the Wilson coefficients a positive (negative) C'_{10} enhances (suppresses) the $B_s \rightarrow \mu^+ \mu^-$ branching ratio while the opposite is true for C_{10}^{NP} . In the ALRS scenario $C'_{10} = -C_{10}^{\text{NP}}$ and taking into account that the data on $\langle F_L \rangle$ and $\langle S_5 \rangle$ require a negative C_9^{NP} implies through (101) an enhancement of $\bar{\mathcal{B}}(B_s \rightarrow \mu^+ \mu^-)$, which could be problematic for ALRS one day.

No such correlation is present in LHS but in this scenario as shown at the beginning of this section, a real C_9^{NP} implies uniquely an enhancement of ΔM_s and $C_{B_s} > 1.00$, which is not favoured by our analysis of $B_{s,d} \rightarrow \mu^+ \mu^-$. Solution to this possible problem are new CP-violating phases and this could be tested in $B_d \rightarrow K^* \mu^+ \mu^-$ by the measurements of the CP-asymmetries A_7 and A_8 .

Finally let us emphasize that the decay $B_d \rightarrow K \mu^+ \mu^-$ can also contribute to this discussion. Indeed the authors of [26] provided an approximate formula for the branching ratio confined to large q^2 region. Lattice calculations of the relevant form factors are making significant progress here [79, 80] and the importance of this decay will increase in the future. For real Wilson coefficients and neglecting the interference between NP contributions the formula of [26] reduces in the absence of NP contributions to Wilson coefficients of dipole operators to

$$10^7 \times \mathcal{B}(B_d \rightarrow K \mu^+ \mu^-)_{[14.2,22]} = 1.11 + 0.27 (C_9^{\text{NP}} + C'_9) - 0.27 (C_{10}^{\text{NP}} + C'_{10}) \quad (102)$$

where the error on the first SM term is estimated to be 10% [79, 80]. This should be compared with the LHCb result

$$10^7 \times \mathcal{B}(B_d \rightarrow K \mu^+ \mu^-)_{[14.2,22]} = 1.04 \pm 0.12 \quad (\text{LHCb}). \quad (103)$$

We can now explicitly see what happens in the four scenarios discussed by us.

- For LHS we find

$$10^7 \times \mathcal{B}(B_d \rightarrow K \mu^+ \mu^-)_{[14.2,22]} = 1.11 + 0.27 (C_9^{\text{NP}} - C_{10}^{\text{NP}}), \quad (104)$$

while for RHS the Wilson coefficients $C_{9,10}^{\text{NP}}$ should be replaced by $C'_{9,10}$. As RHS is not a favourite scenario we will not consider it further.

- For LRS we simply have

$$10^7 \times \mathcal{B}(B_d \rightarrow K \mu^+ \mu^-)_{[14.2,22]} = 1.11 + 0.54 (C_9^{\text{NP}} - C_{10}^{\text{NP}}). \quad (105)$$

In this scenario NP contributions to $B_s \rightarrow \mu^+ \mu^-$ vanish but as seen in this formula they could still be visible in $B_d \rightarrow K \mu^+ \mu^-$ and this is a characteristic feature of this scenario.

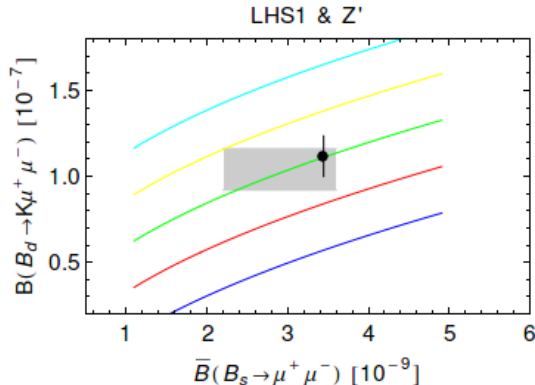


Figure 20: $\mathcal{B}(B_d \rightarrow K\mu^+\mu^-)$ versus $\bar{\mathcal{B}}(B_s \rightarrow \mu^+\mu^-)$ in LHS for different values of C_9^{NP} : -2 (blue), -1 (red), 0 (green), 1 (yellow) and 2 (cyan) and $-0.8 \leq C_{10}^{\text{NP}} \leq 1.8$. The gray area corresponds to the experimental range in (103). SM is represented by the black point.

- The opposite takes place in ALRS where NP contributions to $B_s \rightarrow \mu^+\mu^-$ can be present but vanish for $B_d \rightarrow K\mu^+\mu^-$. In this scenario there is no constraint on angular observables from $B_d \rightarrow K\mu^+\mu^-$.

As stressed in [26] the Wilson coefficient C_9^{NP} by itself has difficulty in removing completely the anomalies in $B_d \rightarrow K^*\mu^+\mu^-$ due to the constraint from $B_d \rightarrow K\mu^+\mu^-$. The LHS scenario allows us to have a closer look at this issue. Using (104) we show in Fig. 20 the correlation between $\mathcal{B}(B_d \rightarrow K\mu^+\mu^-)_{[14.2,22]}$ and $\bar{\mathcal{B}}(B_s \rightarrow \mu^+\mu^-)$ for various values of C_9^{NP} . We show also the $\pm 10\%$ error on SM prediction which should also be taken into account in the lines corresponding to NP predictions with $C_9^{\text{NP}} \neq 0$. Indeed in agreement with [26] only $|C_9^{\text{NP}}| \leq 1.0$ is allowed at 1σ which is insufficient, as seen in Fig. 16, to remove completely $B_d \rightarrow K^*\mu^+\mu^-$ anomalies.

Similarly our recent analysis [74] shows that assuming lepton universality one can derive an upper bound $|C_9^{\text{NP}}| \leq 1.1(1.4)$ from LEP-II data for *all* Z' models with only left-handed flavour violating couplings to quarks when NP contributions to ΔM_s at the level of $10\%(15\%)$ are allowed. In concrete dynamical LHS models, like 331 models analyzed in [74], one even finds $|C_9^{\text{NP}}| \leq 0.8$.

7 Conclusions and outlook

Motivated by recent experimental results on $B_{s,d} \rightarrow \mu^+\mu^-$ and $B \rightarrow K^*\mu^+\mu^-$ we have revisited the LHS scenario of [14] generalizing it to arbitrary $M_{Z'}$, $\bar{\Delta}_A^{\mu\mu}(Z')$ and departures of $(\Delta M_{s,d})_{\text{SM}}$ from the data. This allowed us to present new correlations between various observables. These correlations, shown in many figures will allow in the coming years to monitor whether LHS can describe future more precise data when

also lattice results improve. As already emphasized at the beginning of our paper this will certainly be non-trivial.

Beyond these correlations possibly the most important results of this paper are the following ones:

- LHS provides a simple model that allows for the violation of the CMFV relation between the branching ratios for $B_{d,s} \rightarrow \mu^+\mu^-$ and $\Delta M_{s,d}$. The plots in Figs. 9 and 14 for Z' and Z illustrate this.
- Moreover, LHS is able to accommodate the recent experimental results for $B_{s,d} \rightarrow \mu^+\mu^-$ but this in the case of $\mathcal{B}(B_d \rightarrow \mu^+\mu^-)$ requires $\bar{\Delta}_A^{\mu\bar{\mu}}(Z') \geq 1.0$ and larger by a factor of two relative to the one considered by us in [14].
- The SM Z boson with FCNC couplings to quarks can describe the present data on $B_{s,d} \rightarrow \mu^+\mu^-$ provided ΔM_s and $S_{\psi\phi}$ are very close to their SM values. However, in view of its small vector coupling to muons it cannot describe the anomalies in $B_d \rightarrow K^*\mu^+\mu^-$.
- The explanation of the present anomalies in $B_d \rightarrow K^*\mu^+\mu^-$ with a real $C_9^{\text{NP}}(B_s)$ as proposed in [26, 34] implies uniquely an enhancement of ΔM_s over its SM value. As the present SM value for the ratio $\Delta M_s/\Delta M_d$ agrees with the data very well, it is likely that also ΔM_d should be enhanced in this scenario to agree with experiment. For this pattern to agree with the data the values of the non-perturbative parameters in $\Delta M_{s,d}$ have to be lower than their present central values.
- We have pointed out that the absence of relevant NP contributions to $C_{7\gamma}$ and $C'_{7\gamma}$ in Z' scenarios implies in the limit of negligible new sources of CP violation correlations between the angular observables $\langle F_L \rangle$, $\langle S_4 \rangle$ and $\langle S_5 \rangle$ in LHS, RHS, LRS and ALRS scenarios. In the LHS case there is a unique anti-correlation between $\langle F_L \rangle$ and $\langle S_5 \rangle$, while in the other cases the correlations between any of these two observables depend on the value of $C_9^{\text{NP}}(B_s)$. Eliminating $C_9^{\text{NP}}(B_s)$ in favour of one of these variables results in triple correlations between $\langle F_L \rangle$, $\langle S_4 \rangle$ and $\langle S_5 \rangle$ in RHS, LRS and ALRS scenarios. In LHS NP contributions to $\langle S_4 \rangle$ can be neglected. These correlations depend on hadronic uncertainties which should be significantly reduced before the correlations in question become really useful. Therefore in Appendix A we have presented general formulae for correlations which can be efficiently used in the flavour precision era.
- Our graphical and analytical presentation of correlations between angular observables in $B \rightarrow K^*\mu^+\mu^-$ is complementary to the sophisticated numerical analyses in [26, 34]. Among the four Z' scenarios considered by us ALRS appears to be the favourite scenario followed closely by LHS in agreement with [26]. However the simple LHS, as advocated in [34] and in the dominant part of the present paper could turn out to be the winner when the data and theory will be improved.

- Once the Wilson coefficients C_9^{NP} and C_{10}^{NP} will be determined through $B_s \rightarrow \mu^+\mu^-$, $B \rightarrow K^*\mu^+\mu^-$ and $B \rightarrow K\mu^+\mu^-$ data the $SU(2)_L$ relation in (45) will allow within the LHS model to predict uniquely the $b \rightarrow s\nu\bar{\nu}$ observables. The plot in Fig. 10 illustrates this.

Finally, our analysis has shown how important it is to find out what the values of C_{B_s} and C_{B_d} from lattice calculations are, measure precisely the asymmetries $S_{\psi\phi}$ and $S_{\psi K_S}$ and improve both theoretical and experimental status of all $b \rightarrow s\mu^+\mu^-$ observables discussed by us.

We are looking forward to the flavour precision era in which the simple LHS scenario which dominated our paper will be much better tested than it is possible now. If it fails, the simplest solution would be to introduce right-handed Z' couplings to quarks but as reviewed in [1] this is still another story to which we devoted a short discussion here.

Acknowledgements

We would like to thank Wolfgang Altmannshofer and David Straub for illuminating comments on the status of angular observables and Christoph Bobeth and Cecilia Tarantino for useful informations. This research was financed and done in the context of the ERC Advanced Grant project “FLAVOUR” (267104) with some support from the DFG cluster of excellence ”Origin and Structure of the Universe”.

A General formulae for correlations

In the limit of no new CP-violating phases and neglecting the contributions of dipole operators as well as interferences between NP contributions one can generally write

$$\langle \Delta F_L \rangle \equiv \langle F_L \rangle - \langle F_L \rangle_{\text{SM}} = a_9 C_9^{\text{NP}} + a_{9'} C_9' + a_{10'} C_{10}', \quad (106)$$

$$\langle \Delta S_4 \rangle \equiv \langle S_4 \rangle - \langle S_4 \rangle_{\text{SM}} = b_{9'} C_9' + b_{10'} C_{10}', \quad (107)$$

$$\langle \Delta S_5 \rangle \equiv \langle S_5 \rangle - \langle S_5 \rangle_{\text{SM}} = d_9 C_9^{\text{NP}} + d_{9'} C_9' + d_{10'} C_{10}' . \quad (108)$$

The coefficients a_i , b_i and d_i are subject to hadronic uncertainties. For the form factors used in [26] one has (73)-(75) but as these coefficients will change with time it is useful to present general expressions. In particular one can derive correlations between $\langle \Delta F_L \rangle$, $\langle \Delta S_4 \rangle$ and $\langle \Delta S_5 \rangle$.

In the LHS scenario we simply have

$$\langle \Delta F_L \rangle = \frac{a_9}{d_9} \langle \Delta S_5 \rangle, \quad \langle \Delta S_4 \rangle = 0 . \quad (109)$$

For LR and ALRS scenarios we introduce

$$r_1^\pm = a_9 \pm a_{9'} - \frac{a_{10'}}{d_{10'}}(d_9 \pm d_{9'}) \quad (110)$$

$$r_2^\pm = a_9 \pm a_{9'} \mp \frac{a_{10'}}{b_{10'}}b_{9'} \quad (111)$$

with $r_{1,2}^+$ for LRS and $r_{1,2}^-$ for ALRS.

Then we find the correlations

$$\langle \Delta F_L \rangle = \frac{a_{10'}}{d_{10'}} \langle \Delta S_5 \rangle + r_1^\pm C_9^{\text{NP}} \quad (112)$$

$$\langle \Delta F_L \rangle = \frac{a_{10'}}{b_{10'}} \langle \Delta S_4 \rangle + r_2^\pm C_9^{\text{NP}} \quad (113)$$

and the triple correlation

$$\left(1 - \frac{r_1^\pm}{r_2^\pm}\right) \langle \Delta F_L \rangle = \frac{a_{10'}}{d_{10'}} \langle \Delta S_5 \rangle - \frac{r_1^\pm a_{10'}}{r_2^\pm b_{10'}} \langle \Delta S_4 \rangle. \quad (114)$$

In the RHS scenario one should set $a_9 = d_9 = 0$ and $C_9^{\text{NP}} = C_9'$ in this formulae and use $r_{1,2}^+$.

Inserting the numerical values for a_i , b_i and d_i given in (73)-(75) into these formulae one recovers the correlations used in our numerical analysis.

References

- [1] A. J. Buras and J. Girrbach, *Towards the Identification of New Physics through Quark Flavour Violating Processes*, [arXiv:1306.3775](#).
- [2] A. J. Buras, P. Gambino, M. Gorbahn, S. Jager, and L. Silvestrini, *Universal unitarity triangle and physics beyond the standard model*, *Phys. Lett.* **B500** (2001) 161–167, [[hep-ph/0007085](#)].
- [3] A. J. Buras, *Minimal flavor violation*, *Acta Phys. Polon.* **B34** (2003) 5615–5668, [[hep-ph/0310208](#)].
- [4] R. S. Chivukula and H. Georgi, *Composite technicolor standard model*, *Phys. Lett.* **B188** (1987) 99.
- [5] L. J. Hall and L. Randall, *Weak scale effective supersymmetry*, *Phys. Rev. Lett.* **65** (1990) 2939–2942.
- [6] G. D’Ambrosio, G. F. Giudice, G. Isidori, and A. Strumia, *Minimal flavour violation: An effective field theory approach*, *Nucl. Phys.* **B645** (2002) 155–187, [[hep-ph/0207036](#)].

-
- [7] A. L. Kagan, G. Perez, T. Volansky, and J. Zupan, *General Minimal Flavor Violation*, *Phys.Rev.* **D80** (2009) 076002, [arXiv:0903.1794].
- [8] R. Barbieri, G. Isidori, J. Jones-Perez, P. Lodone, and D. M. Straub, *$U(2)$ and Minimal Flavour Violation in Supersymmetry*, *Eur.Phys.J.* **C71** (2011) 1725, [arXiv:1105.2296].
- [9] R. Barbieri, D. Buttazzo, F. Sala, and D. M. Straub, *Flavour physics from an approximate $U(2)^3$ symmetry*, *JHEP* **1207** (2012) 181, [arXiv:1203.4218].
- [10] A. Crivellin, L. Hofer, and U. Nierste, *The MSSM with a Softly Broken $U(2)^3$ Flavor Symmetry*, *PoS EPS-HEP2011* (2011) 145, [arXiv:1111.0246].
- [11] A. J. Buras and J. Girrbach, *On the Correlations between Flavour Observables in Minimal $U(2)^3$ Models*, *JHEP* **1301** (2013) 007, [arXiv:1206.3878].
- [12] W. Altmannshofer, A. J. Buras, S. Gori, P. Paradisi, and D. M. Straub, *Anatomy and Phenomenology of FCNC and CPV Effects in SUSY Theories*, *Nucl.Phys.* **B830** (2010) 17–94, [arXiv:0909.1333].
- [13] A. J. Buras, F. De Fazio, J. Girrbach, and M. V. Carlucci, *The Anatomy of Quark Flavour Observables in 331 Models in the Flavour Precision Era*, *JHEP* **1302** (2013) 023, [arXiv:1211.1237].
- [14] A. J. Buras, F. De Fazio, and J. Girrbach, *The Anatomy of Z' and Z with Flavour Changing Neutral Currents in the Flavour Precision Era*, *JHEP* **1302** (2013) 116, [arXiv:1211.1896].
- [15] A. J. Buras, J. Girrbach, and R. Ziegler, *Particle-Antiparticle Mixing, CP Violation and Rare K and B Decays in a Minimal Theory of Fermion Masses*, *JHEP* **1304** (2013) 168, [arXiv:1301.5498].
- [16] A. J. Buras, R. Fleischer, J. Girrbach, and R. Knegjens, *Probing New Physics with the $B_s \rightarrow \mu^+ \mu^-$ Time-Dependent Rate*, *JHEP* **1307** (2013) 77, [arXiv:1303.3820].
- [17] A. J. Buras, F. De Fazio, J. Girrbach, R. Knegjens, and M. Nagai, *The Anatomy of Neutral Scalars with FCNCs in the Flavour Precision Era*, *JHEP* **1306** (2013) 111, [arXiv:1303.3723].
- [18] P. Langacker, *The Physics of Heavy Z' Gauge Bosons*, *Rev.Mod.Phys.* **81** (2009) 1199–1228, [arXiv:0801.1345].
- [19] V. Barger, L. L. Everett, J. Jiang, P. Langacker, T. Liu, *et. al.*, *$b \rightarrow s$ Transitions in Family-dependent $U(1)'$ Models*, *JHEP* **0912** (2009) 048, [arXiv:0906.3745].
- [20] P. J. Fox, J. Liu, D. Tucker-Smith, and N. Weiner, *An Effective Z'* , *Phys.Rev.* **D84** (2011) 115006, [arXiv:1104.4127].

-
- [21] W. Altmannshofer, P. Paradisi, and D. M. Straub, *Model-Independent Constraints on New Physics in $b \rightarrow s\gamma$ Transitions*, *JHEP* **1204** (2012) 008, [[arXiv:1111.1257](#)].
- [22] W. Altmannshofer and D. M. Straub, *Cornering New Physics in $b \rightarrow s$ Transitions*, *JHEP* **1208** (2012) 121, [[arXiv:1206.0273](#)].
- [23] A. Dighe and D. Ghosh, *How large can the branching ratio of $B_s \rightarrow \tau^+\tau^-$ be ?*, *Phys.Rev.* **D86** (2012) 054023, [[arXiv:1207.1324](#)].
- [24] S. Sun, D. B. Kaplan, and A. E. Nelson, *Little flavor: A model of weak-scale flavor physics*, *Phys.Rev.* **D87** (2013) 125036, [[arXiv:1303.1811](#)].
- [25] A. J. Buras, *Relations between $\Delta M_{s,d}$ and $B_{s,d} \rightarrow \mu^+\mu^-$ in models with minimal flavour violation*, *Phys. Lett.* **B566** (2003) 115–119, [[hep-ph/0303060](#)].
- [26] W. Altmannshofer and D. M. Straub, *New physics in $B \rightarrow K^*\mu\mu$?*, [arXiv:1308.1501](#).
- [27] R. Gauld, F. Goertz, and U. Haisch, *On minimal Z' explanations of the $B \rightarrow K^*\mu^+\mu^-$ anomaly*, [arXiv:1308.1959](#).
- [28] **LHCb collaboration** Collaboration, R. Aaij *et. al.*, *Measurement of the $B_s^0 \rightarrow \mu^+\mu^-$ branching fraction and search for $B^0 \rightarrow \mu^+\mu^-$ decays at the LHCb experiment*, [arXiv:1307.5024](#).
- [29] **CMS Collaboration** Collaboration, S. Chatrchyan *et. al.*, *Measurement of the $B_s \rightarrow \mu\mu$ branching fraction and search for $B_0 \rightarrow \mu\mu$ with the CMS Experiment*, [arXiv:1307.5025](#).
- [30] *Combination of results on the rare decays $b \rightarrow \mu^+\mu^-$ from the cms and lhcb experiments*, Tech. Rep. CMS-PAS-BPH-13-007, CERN, Geneva, 2013.
- [31] **LHCb Collaboration** Collaboration, R. Aaij *et. al.*, *Differential branching fraction and angular analysis of the decay $B^0 \rightarrow K^{*0}\mu^+\mu^-$* , [arXiv:1304.6325](#).
- [32] **LHCb collaboration** Collaboration, R. Aaij *et. al.*, *Measurement of form-factor independent observables in the decay $B^0 \rightarrow K^{*0}\mu^+\mu^-$* , [arXiv:1308.1707](#).
- [33] **CMS Collaboration** Collaboration, S. Chatrchyan *et. al.*, *Angular analysis and branching fraction measurement of the decay $B^0 \rightarrow K^*\mu^+\mu^-$* , [arXiv:1308.3409](#).
- [34] S. Descotes-Genon, J. Matias, and J. Virto, *Understanding the $B \rightarrow K^*\mu^+\mu^-$ Anomaly*, *Phys. Rev. D* **88**, **074002** (2013) [[arXiv:1307.5683](#)].
- [35] A. Khodjamirian, T. Mannel, A. Pivovarov, and Y.-M. Wang, *Charm-loop effect in $B \rightarrow K^{(*)}\ell^+\ell^-$ and $B \rightarrow K^*\gamma$* , *JHEP* **1009** (2010) 089, [[arXiv:1006.4945](#)].

-
- [36] M. Beylich, G. Buchalla, and T. Feldmann, *Theory of $B \rightarrow K^{(*)}l^+l^-$ decays at high q^2 : OPE and quark-hadron duality*, *Eur.Phys.J.* **C71** (2011) 1635, [arXiv:1101.5118].
- [37] J. Matias, *On the S-wave pollution of $B \rightarrow K^*l^+l^-$ observables*, *Phys.Rev.* **D86** (2012) 094024, [arXiv:1209.1525].
- [38] S. Jager and J. M. Camalich, *On $B \rightarrow V\ell\ell$ at small dilepton invariant mass, power corrections, and new physics*, *JHEP* **1305** (2013) 043, [arXiv:1212.2263].
- [39] D. Guadagnoli and G. Isidori, *$BR(B_s \rightarrow \mu^+\mu^-)$ as an electroweak precision test*, arXiv:1302.3909.
- [40] A. J. Buras and J. Girrbach, *Complete NLO QCD Corrections for Tree Level Delta $F = 2$ FCNC Processes*, *JHEP* **1203** (2012) 052, [arXiv:1201.1302].
- [41] A. J. Buras, M. Jamin, and P. H. Weisz, *Leading and next-to-leading QCD corrections to ε parameter and $B^0 - \bar{B}^0$ mixing in the presence of a heavy top quark*, *Nucl. Phys.* **B347** (1990) 491–536.
- [42] C. Bobeth, P. Gambino, M. Gorbahn, and U. Haisch, *Complete NNLO QCD analysis of $\bar{B} \rightarrow X_s\ell^+\ell^-$ and higher order electroweak effects*, *JHEP* **04** (2004) 071, [hep-ph/0312090].
- [43] T. Huber, E. Lunghi, M. Misiak, and D. Wyler, *Electromagnetic logarithms in $\bar{B} \rightarrow X(s)l^+l^-$* , *Nucl.Phys.* **B740** (2006) 105–137, [hep-ph/0512066].
- [44] A. J. Buras and M. Munz, *Effective hamiltonian for $b \rightarrow x_s e^+e^-$ beyond leading logarithms in the ndr and hv schemes*, *Phys. Rev.* **D52** (1995) 186–195, [hep-ph/9501281].
- [45] C. Bobeth, M. Misiak, and J. Urban, *Photonic penguins at two loops and m_t -dependence of $BR(B \rightarrow X_s\ell^+\ell^-)$* , *Nucl. Phys.* **B574** (2000) 291–330, [hep-ph/9910220].
- [46] C. Bobeth, M. Misiak, and J. Urban, *Matching conditions for $b \rightarrow s\gamma$ and $b \rightarrow sg$ in extensions of the standard model*, *Nucl.Phys.* **B567** (2000) 153–185, [hep-ph/9904413].
- [47] A. J. Buras, L. Merlo, and E. Stamou, *The Impact of Flavour Changing Neutral Gauge Bosons on $\bar{B} \rightarrow X_s\gamma$* , *JHEP* **1108** (2011) 124, [arXiv:1105.5146].
- [48] K. De Bruyn, R. Fleischer, R. Knegjens, P. Koppenburg, M. Merk, *et. al.*, *Probing New Physics via the $B_s^0 \rightarrow \mu^+\mu^-$ Effective Lifetime*, *Phys.Rev.Lett.* **109** (2012) 041801, [arXiv:1204.1737].

- [49] R. Fleischer, *On Branching Ratios of B_s Decays and the Search for New Physics in $B_s^0 \rightarrow \mu^+\mu^-$* , *Nucl.Phys.Proc.Suppl.* **241-242** (2013) 135–140, [arXiv:1208.2843].
- [50] A. J. Buras, J. Girrbach, D. Guadagnoli, and G. Isidori, *On the Standard Model prediction for $BR(B_{s,d} \rightarrow \mu^+\mu^-)$* , *Eur.Phys.J.* **C72** (2012) 2172, [arXiv:1208.0934].
- [51] F. Beaujean, C. Bobeth, D. van Dyk, and C. Wacker, *Bayesian Fit of Exclusive $b \rightarrow s\ell\ell$ Decays: The Standard Model Operator Basis*, *JHEP* **1208** (2012) 030, [arXiv:1205.1838].
- [52] C. Bobeth, G. Hiller, and D. van Dyk, *General Analysis of $\bar{B} \rightarrow \bar{K}^{(*)}\ell^+\ell^-$ Decays at Low Recoil*, *Phys.Rev.* **D87** (2013) 034016, [arXiv:1212.2321].
- [53] F. Beaujean, C. Bobeth, and D. van Dyk, *Comprehensive Bayesian Analysis of Rare (Semi)leptonic and Radiative B Decays*, arXiv:1310.2478.
- [54] R. R. Horgan, Z. Liu, S. Meinel, and M. Wingate, *Calculation of $B^0 \rightarrow K^{*0}\mu^+\mu^-$ and $B_s^0 \rightarrow \phi\mu^+\mu^-$ observables using form factors from lattice QCD*, arXiv:1310.3887.
- [55] G. Colangelo, S. Durr, A. Juttner, L. Lellouch, H. Leutwyler, *et. al.*, *Review of lattice results concerning low energy particle physics*, *Eur.Phys.J.* **C71** (2011) 1695, [arXiv:1011.4408].
- [56] T. Hurth, G. Isidori, J. F. Kamenik, and F. Mescia, *Constraints on New Physics in MFV models: A Model-independent analysis of $\Delta F = 1$ processes*, *Nucl. Phys.* **B808** (2009) 326–346, [arXiv:0807.5039].
- [57] N. Carrasco, M. Ciuchini, P. Dimopoulos, R. Frezzotti, V. Gimenez, *et. al.*, *B-physics from $N_f=2$ tmQCD: the Standard Model and beyond*, arXiv:1308.1851.
- [58] J. Laiho, E. Lunghi, and R. S. Van de Water, *Lattice QCD inputs to the CKM unitarity triangle analysis*, *Phys. Rev.* **D81** (2010) 034503, [arXiv:0910.2928]. Updates available on <http://latticeaverages.org/>.
- [59] A. J. Buras and J. Girrbach, *Stringent Tests of Constrained Minimal Flavour Violation through $\Delta F = 2$ Transitions*, *The European Physical Journal C* **9** (73) 2013, [arXiv:1304.6835].
- [60] W. Marciano and A. Sirlin, *Constraint on additional neutral gauge bosons from electroweak radiative corrections*, *Phys.Rev.* **D35** (1987) 1672–1676.
- [61] W. Altmannshofer, A. J. Buras, D. M. Straub, and M. Wick, *New strategies for New Physics search in $B \rightarrow K^*\nu\bar{\nu}$, $B \rightarrow K\nu\bar{\nu}$ and $B \rightarrow X_s\nu\bar{\nu}$ decays*, *JHEP* **04** (2009) 022, [arXiv:0902.0160].

- [62] **Heavy Flavor Averaging Group** Collaboration, Y. Amhis *et. al.*, *Averages of B-Hadron, C-Hadron, and tau-lepton properties as of early 2012*, [arXiv:1207.1158](#).
- [63] **LHCb collaboration** Collaboration, R. Aaij *et. al.*, *Measurement of CP violation and the B_s^0 meson decay width difference with $B_s^0 \rightarrow J/\psi K^+ K^-$ and $B_s^0 \rightarrow J/\psi \pi^+ \pi^-$ decays*, [arXiv:1304.2600](#).
- [64] **UTfit** Collaboration, M. Bona *et. al.*, *The UTfit collaboration report on the unitarity triangle beyond the standard model: Spring 2006*, *Phys. Rev. Lett.* **97** (2006) 151803, [[hep-ph/0605213](#)]. Updates available on <http://www.utfit.org>.
- [65] D. M. Straub, *Constraints on new physics from rare (semi-)leptonic B decays*, [arXiv:1305.5704](#).
- [66] W. Altmannshofer, *The $B_s \rightarrow \mu^+ \mu^-$ and $B_d \rightarrow \mu^+ \mu^-$ Decays: Standard Model and Beyond*, [arXiv:1306.0022](#).
- [67] P. Colangelo, F. De Fazio, P. Santorelli, and E. Scrimieri, *Rare $B \rightarrow K^{(*)} \nu \bar{\nu}$ decays at B factories*, *Phys.Lett.* **B395** (1997) 339–344, [[hep-ph/9610297](#)].
- [68] G. Buchalla, G. Hiller, and G. Isidori, *Phenomenology of non-standard Z couplings in exclusive semileptonic $b \rightarrow s$ transitions*, *Phys. Rev.* **D63** (2001) 014015, [[hep-ph/0006136](#)].
- [69] M. Blanke, A. J. Buras, B. Duling, S. Recksiegel, and C. Tarantino, *FCNC Processes in the Littlest Higgs Model with T-Parity: a 2009 Look*, *Acta Phys.Polon.* **B41** (2010) 657–683, [[arXiv:0906.5454](#)].
- [70] O. Eberhardt, G. Herbert, H. Lacker, A. Lenz, A. Menzel, *et. al.*, *Impact of a Higgs boson at a mass of 126 GeV on the standard model with three and four fermion generations*, *Phys.Rev.Lett.* **109** (2012) 241802, [[arXiv:1209.1101](#)].
- [71] A. J. Buras, B. Duling, T. Feldmann, T. Heidsieck, C. Promberger, *et. al.*, *Patterns of Flavour Violation in the Presence of a Fourth Generation of Quarks and Leptons*, *JHEP* **1009** (2010) 106, [[arXiv:1002.2126](#)].
- [72] G. W. S. Hou, *Enhanced $B_d \rightarrow \mu^+ \mu^-$ Decay: What if?*, [arXiv:1307.2448](#).
- [73] M. Blanke, A. J. Buras, B. Duling, K. Gemmler, and S. Gori, *Rare K and B Decays in a Warped Extra Dimension with Custodial Protection*, *JHEP* **03** (2009) 108, [[arXiv:0812.3803](#)].
- [74] A. J. Buras, F. De Fazio, and J. Girrbach, *331 models facing new $b \rightarrow smu^+ mu^-$ data*, [arXiv:1311.6729](#).

-
- [75] **ALEPH Collaboration, DELPHI Collaboration, L3 Collaboration, OPAL Collaboration, LEP Electroweak Working Group Collaboration,** S. Schael *et. al.*, *Electroweak Measurements in Electron-Positron Collisions at W-Boson-Pair Energies at LEP*, [arXiv:1302.3415](#).
- [76] W. Altmannshofer, P. Ball, A. Bharucha, A. J. Buras, D. M. Straub, *et. al.*, *Symmetries and Asymmetries of $B \rightarrow K^* \mu^+ \mu^-$ Decays in the Standard Model and Beyond*, *JHEP* **0901** (2009) 019, [[arXiv:0811.1214](#)].
- [77] S. Descotes-Genon, T. Hurth, J. Matias, and J. Virto, *Optimizing the basis of $B \rightarrow K^* \ell^+ \ell^-$ observables in the full kinematic range*, *JHEP* **1305** (2013) 137, [[arXiv:1303.5794](#)].
- [78] C. Hambrock, G. Hiller, S. Schacht, and R. Zwicky, *$B \rightarrow K^*$ Form Factors from Flavor Data to QCD and Back*, [arXiv:1308.4379](#).
- [79] C. Bouchard, G. P. Lepage, C. Monahan, H. Na, and J. Shigemitsu, *Standard Model predictions for $B \rightarrow K \ell \ell$ with form factors from lattice QCD*, *Phys. Rev. Lett.* **111**, **162002** (2013) [[arXiv:1306.0434](#)].
- [80] C. Bouchard, G. P. Lepage, C. Monahan, H. Na, and J. Shigemitsu, *Rare decay $B \rightarrow K \ell \ell$ form factors from lattice QCD*, *Phys. Rev. D* **88**, **054509** (2013) 054509, [[arXiv:1306.2384](#)].